Peer-reviewed version available at Atmosphere 2018, 9, 288; doi:10.3390/atmos9080288

Article

Analysis of Dust Aerosol Retrievals using Satellite Data in Central Asia

Longlei Li [1,*], Irina N. Sokolik [1]

[1] School of Earth and Atmospheric Sciences, Georgia Institute of Technology, Atlanta, GA, USA; l.longlei@gmail.com (L.L.); isokolik@eas.gatech.edu (I.N.S.)
* Correspondence: l.longlei@gmail.com; Tel.: +01-404-754-1177

Abstract: Several long-term monitoring of aerosol datasets from the Moderate Resolution Imaging Spectroradiometer (MODIS) on board Terra/Aqua, Multi-angle Imaging SpectroRadiometer (MISR), Sea-Viewing Wide Field-of-View Sensor (SeaWiFS) are used to derive the dust aerosol optical depth (DOD) in Central Asia based on the Angstrom exponent parameter and/or the particle shape. All sensors agree very well on the interannual variability of DOD. The seasonal analysis of DOD and dust occurrences identified the largest dust loading and the most frequent dust occurrence in the spring and summer, respectively. No significant trend is found during the research period in terms of both DOD and the dust occurrence. Further analysis of Cloud-Aerosol Lidar and Infrared Pathfinder Satellite Observation (CALIPSO) aerosol products on a case-by-case basis in most dust months of 2007 suggested that the vertical structure is varying in terms of the extension and the dust loading from one event to another, although dust particles of most episodes have similar physical characteristics (the particle shape and size). Our analysis on the vertical structure of dust plumes, the layer-integrated color ratio and depolarization ratio indicates a varied climate effect (e.g., the direct radiative impact) by mineral dust, dependent on the event being observed in Central Asia.

Keywords: dust aerosol; Central Asia; remote sensing; seasonal variation; inter-annual variability

1. Introduction

Mineral dust is one of the most abundant aerosols on the Earth. Mineral dust may affect the climate system by interacting with the atmospheric radiation [1], with the ecosystems [2], and with the cloud microphysics [3]. Accurately quantifying these effects by mineral dust, however, is still one of the major scientific problems at both global and regional scales. Once lifting into the atmosphere, dust aerosols experience a variety of physical and chemical processes. The crucial things of exploring these issues include accurately quantifying the dust loading in the fine mode (for estimating the direct radiative effect) and in the coarse mode (for studies on its role in the cloud formation, as well as the radiative effects), measuring chemical compositions, determining transport pathways and the deposition intensity (e.g., for studies on the iron supply to the ecosystem), and studying vertical structures (for radiative and cloud microphysical effects). Thus, studies on the dust occurrence and the vertical structure are of great importance to understand the role of dust in the human-climate-environment system.

Numerous publications documented the dust occurrence in Africa and East Asian deserts, two main dust sources, but few studies exist addressing this issue in Central Asia. Central Asia consists of five countries: southern Kazakhstan, Turkmenistan, Uzbekistan, Kygryzstan, Tajikistan, Pakistan. Mineral dust in Central Asia is mainly found along the "dust belt" from the eastern Caspian Sea, through the Ustyurt Plateau and the Aral Kum Deserts to the Balqash Lake [4] The Aral Kum is a newly formed dust source caused by the desiccation of the Aral Sea. Approximately 7.5×10^6 tons of dust are blown out of the desert annually [5] rendering it to be one of the most important dust sources worldwide. Dust particles from this region can be carried away to distance of thousands of kilometers to northern Iran, as revealed by images from the Advanced very-high-resolution

radiometer (AVHRR) [6]. Only a small fraction of dust occurrence can have a long-range transport, one branch northeastward into the north of Mongolia (a frequency of 9%) and the other into the Central Russia (a frequency of 13%) during spring seasons [7]. Existing publications suggest that the dust occurrence in this region has contributed to the surface heating of the Aral Sea, to the energetic cyclone activity, and the cold wave intrusions during warm seasons [8]. Thus, monitoring and documenting the dust occurrence characteristic and intensity, dust sources, and its transport are urgently needed both from the environmental and climatic perspectives so that governments of these regions can make appropriate decisions to prevent dust adverse impacts. Most available studies that address the development of dust storms in Central Asia [6] like Turkmenistan [9] and the Aral Sea Basin [10] were limited by the short period of the observations (less than a decade) and/or the amount of available data on the deposition, the visibility, and the absorbing index (AI). Furthermore, to gain the dust occurrence in the atmosphere indirectly from the dust deposition measurement is very difficult due to the lack of transport information. Analysis of Indoitu et al. [6] is also suffered from the height-dependence problem of the AI products [11], although the dependence might be not that strong in this region due to small AI values. In addition to the very short period (2005-2008), contributions from non-dust absorbing aerosols like biomass burning, which produces AI almost as high as dust plumes, are not excluded.

Satellite remote sensed Aerosol Optical Depth (AOD) is the most useful information available to characterize dust activities over source regions, especially in Central Asia where few ground-based observations are available and modeling dust emissions are still challenging on both daily and monthly basis [4]. The use of satellite sensing AOD has been increasing in the last decade to quantify aerosols over a specific region or around the globe [12,13]. Evaluation work [14,15] has shown that the Multi-angle Imaging Spectro-Radiometer (hereafter referred to as MISR) AOD is in general consistent with ground-based observations within 20% of the AOD in desert areas, although it substantially underestimated for cases with AOD > 0.5 in China [16]. The Moderate Resolution Imaging Spectroradiometer (referred as MODIS hereafter) AOD is also well correlated with the Aerosol Robotic Network (AERONET) measurements in general around the globe [17]. Here aerosol products from several satellite sensors, MODIS on board Terra and Aqua, Ozone Monitoring Instrument (OMI), MISR, and Sea-Viewing Wide Field-of-View Sensor (SeaWiFS) are analyzed. MODIS aerosol product provides a useful tool to monitor dust occurrence and to evaluate the model performance of simulating dust from regional to global scales, although it overpassed a specific site once per day. The L2 aerosol product has a very high spatial resolution (10 km × 10 km), which is helpful to quantify dust characteristics. In 2004, Hsu et al. [18] extended the retrieval of AOD at 550 nm from the dark target (ocean and dense vegetation-covered land surfaces) to the relative bright surface types like bare soil types, taking the advantage of the multiple radiances (especially at 412 nm) measured by the MODIS sensor. Based on the newly developed product, Ginoux et al. [19] designed a simple algorithm by calculating the dust frequency of occurrence (FOO) to try to identify the anthropogenic and nature dust sources. OMI Aerosol Index (AI) along with its predecessor, TOMS (TOtal Ozone Mapping Spectrometer) AI, is another commonly used satellite remote sensing product to obtain the information on dust aerosols and their sources [20-22], although it has a rough spatial resolution (averaged 100km and 50km at nadir, horizontally) and it is sensitive to the aerosol layer height [11]. In addition, the use of the Cloud-Aerosol Lidar and Infrared Pathfinder Satellite Observations (CALIPSO) offers an opportunity to measure the vertical distribution of aerosols. For example, using the CALIPSO and surface measurements, Huang et al. [23] found that dust aerosols originating from the source regions of the Taklimakan and Gobi Deserts may undergo the long-range transport via upper tropospheric westerly jets where dust might impose a long-lasting impact on the climate due to the extended lifetime. Utilizing the CALIPSO lidar data, Liu et al. [24] examined a long-distance transport across the Atlantic Ocean to the Gulf of Mexico for a dust storm case in North Africa on August 17, 2006.

The goal of this study is to characterize the spatial, inter-annual, and seasonal variation of dust aerosol properties in Central Asia based on satellite retrievals over a long-term period (2000-2016). We will further confirm results from the existing literature and show whether there are significant

differences among aforementioned sensors on these issues. To fulfill this goal, MODIS, the Level 2, Collection 6 swath data are used with a horizontal resolution of 10 km × 10 km at nadir, including spectral AOD, the fraction of AOD from particles in the fine mode to total AOD, and the Angstrom parameter over the entire area of Central Asia for 2000-2016. For MISR, Level 2 swath data are utilized with the horizontal resolution of 17.6 km × 17.6 km, covering a period from 2003 to 2016. For SeaWiFS, the swath data of Level 2 from 2000 to 2010 are used. This work is among the first systematical dust climatology studies over Central Asia employing the prevailing long-term satellite datasets. The radiative effect of dust is highly dependent on the vertical structure of dust layers [25-27]. The vertical distribution, especially relative to the cloud, is vital to estimating the impact of mineral dust on the cloud microphysics, as well as the dust radiative impact. Numerous observations with both in-situ measurements and satellite remote sensing (lidar) have been performed to study the vertical dust profiles in east Asia [23], north Africa [28], and Mediterranean [29] moving toward the Atlantic [30-32] and the Pacific Ocean [33]. However, there are no studies available, to the best of our knowledge, that examine dust over the Central Asia region. Thus, this study also presents the dust radiative properties using the CALIPSO instrument (Vertical Feature Mas and the total backscatter coefficient at 532 nm) based on several dust storm cases, e.g., the ones that occurred on May 7, 2007. Our analysis also includes one of the important East Asia dust sources, the Taklimakan Desert, for a comparison purpose.

2. The Study Domain

Our study domain is the Central Asia region (Figure 1) that is bounded by the western China to the east, the southern to the north, the Caspian Sea to the west, and the mountain range in Iran, Afghanistan, and Pakistan to the south. The annual amount of rainfall ranges from $\mathbf{80mm - 200mm}$ (maximum in the spring) and is less than 100 mm in most desert regions (e.g., Kara Kum, Kyzyl Kum, Betpak-Dala). It has a distinct climate contract between northern and southern parts: cold and dry continental climate in the north (mean annual temperatures: $\mathbf{5}℃ - \mathbf{11}℃$), but hot and dry Mediterranean climate in the south (mean annual temperatures: $\mathbf{13}℃ - \mathbf{17}℃$). Deserts in Central Asia are different from other regions like North Africa where few human activities occur. Human plays an important role in the formation of deserts in Central Asia. Retreating of the Aral Sea has begun in the 1960s due to a combination effect of agricultural activities, an expansion of the irrigated area (increasing by 40.6% from 1918 to 1960), and regional climate changes. Particularly, during the first decade of the 21st century, the retreating of the Aral Sea was accelerating (the desiccation process has been successfully captured by the MODIS true color images). Thus, the exposed bottom becomes the so-called Aral Kum Desert, covering more than 57, 500 $\mathbf{km^2}$ by area in August 2011 [34]. It turns to be a powerful source of dust and salt emissions. For instance, an estimation based on the WRF-Chem (Weather Research and Forecasting coupled with Chemistry) model indicates that this area contributes approximately 12% to the total dust emissions of this area by mass in April during 2000-2014 [4]. An "ideal" dust storm that occurred over this area was on May 7, May 8, and May 9, 2007 (lasting three days) due to a cyclone system. This event was also successfully captured by the MODIS true color image, as shown in Figure 5 of Li and Sokolik [35] and the AVHRR image [6].

Preprints (www.preprints.org) | NOT PEER-REVIEWED | Posted: 11 June 2018 doi:10.20944/preprints201806.0158.v1

Peer-reviewed version available at Atmosphere 2018, 9, 288; doi:10.3390/atmos9080288

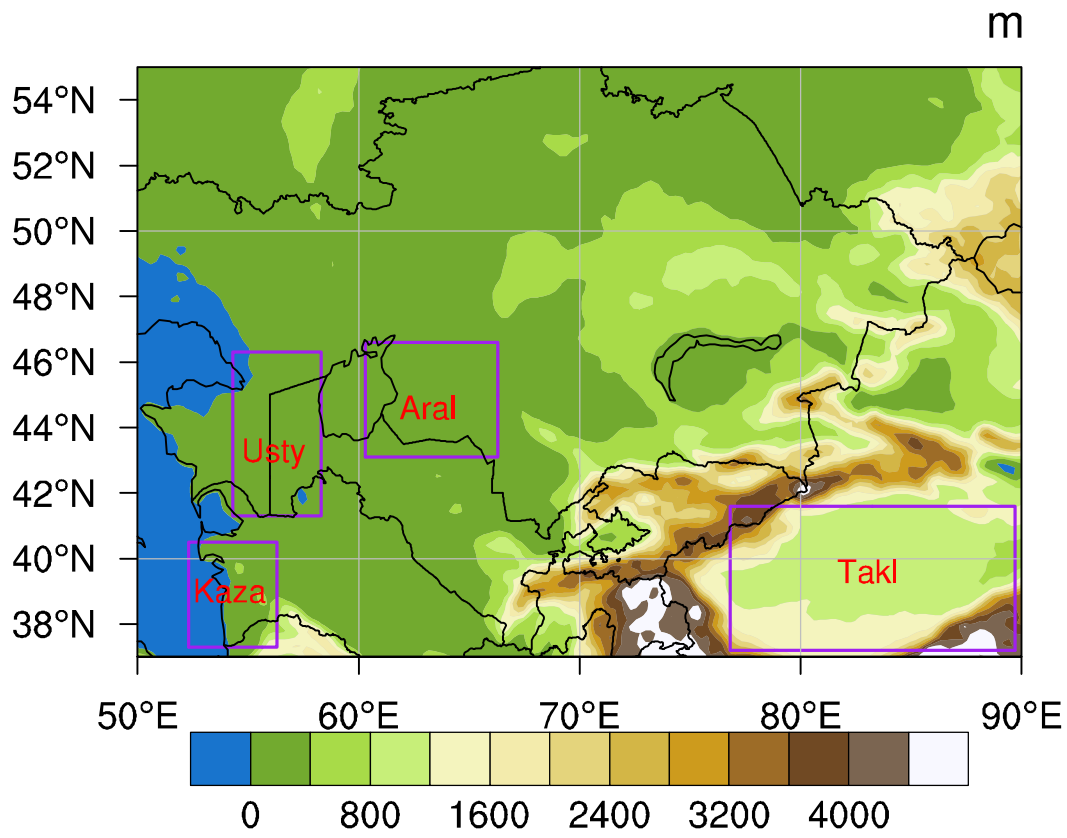

Figure 1. The research domain, Central Asia and its topography (shading area, unit: m). Purple boxes represent four sub-regions where statistical analysis will be applied in the following sections. We use Kaza refer to the area surrounding Kazandzhik and use Usty, Aral, and Takl, refer to the Ustyurt Plateau, the Aral Kum Desert, and the Taklimakan Desert, respectively.

3. Data

3.1 MODIS AOD

MODIS was launched in 1999 in the Terra constellation. MODIS AOD over bright regions is obtained by best fitting the reflectance database based on its geo-location to the simulated lookup table consisting of observation angles, surface reflectance, AOD, and aerosol radiative properties at deep blue (412 nm), 490 nm, and 670 nm (Deep Blue Algorithm) for each retrieval pixel [18] (Hsu et al., 2004). The pixel AOD is then averaged over a 10 km × 10 km cell (at nadir) to obtain the released product (Level 2 Collection 6 MODIS AOD), swath granules consisting of approximately 1500 × 2000 such cells (swath width: 2,300 km). To produce AOD statistics, we remap these granules onto 20 km × 20 km regular grids and averaged all granules from the same grid to form a daily value. Although the MODIS AOD has a regular gridded data (Level 3), the spatial resolution of this dataset is too rough (**1**° × **1**°) to use for regional studies. During the data processing, we avoid remapping onto a much finer grid because the interpolation algorithm would lead to an additional error. The remapping and averaging method is repeated for every day of the eight months (March-November) from 2000 to 2016.

The Deep Blue Algorithm screens out pixels with cloud contaminations. The main uncertainties of the AOD retrievals are due to the cloud processing, measured surface reflectance, and some assumptions on the complex refractive indices, the particle shape, the vertical profile, and the particle size distribution. The spherical assumption leads to an error as large as 40% in the phase function calculation [36]. It would likely reduce the amount of retrieved pixels yielding an underestimation of AOD. Because the most dust occurrence in Central Asia is due to high-pressure systems and only

some associated with cyclones, the cloud-contamination is not a great problem. The sensitivity test on the vertical profile shows that an error of 2 km in the altitude results in the AOD of 25% at 412 nm and 5% at 490 nm [18]. The vertical extension of the dust layer in Central Asia is within 3 km for the most dust occurrence (see further discussions of this issue in Section 5 based on the CALIPSO product). Thus, the error associated with the vertical profile assumption in the algorithm is negligible for Central Asia and the overall uncertainty of retrieving AOD using this algorithm should be less than the reported value at 550 nm.

3.2 SeaWiFS AOD

SeaWiFS has a spatial footprint of approximately $\mathbf{13.5\ km \times 13.5\ km}$, resulting from the averaging of 3×3 pixel with each $\mathbf{4.5\ km \times 4.5\ km}$. Its sampling time is from the noon to the early afternoon in between Terra and Aqua satellites. The aerosol products of Version 003, Level 3 gridded composite at a spatial resolution of $\mathbf{0.5° \times 0.5°}$ are used here. The over-land AOD retrieval from this product is also based on the Deep Blue Algorithm, as used by MODIS over-land AOD dataset. This dataset provides AOD at the commonly-used reference wavelength of 550 nm with a valid range of 0-5 from an arithmetic mean of data with confidence flag equal to 3, directly available through the parameter "aerosol_optical_thickness_550_land". The basic principle for the AOD retrieval over land is the same as MODIS, but has two distinguish developments. Firstly, SeaWiFS has been expanded to include the vegetated surfaces in addition to the bright arid land, and, secondly, it employed a more sophisticated handling with the surface reflectance dataset based on the stratified Lambertian-equivalent reflectivity (LER) for a specific location by the viewing geometry to account for surface bidirectional reflectance distribution function (BRDF) effects. The AOD dataset used here has a time spanning from 2000 to 2010, although SeaWiFS was in operation between September 1997 and December 2010, as the MODIS AOD dataset has been available since 2000.

3.3 MISR AOD

MISR is another instrument observing the Earth on the Terra platform orbiting the polar at an altitude of 705 km. It uses nine cameras (having 36 channels in total) that are fixed at particular view zenith angles ($\mathbf{0°, 26.1°, 45.6°, 60.0°, and\ 70.5°}$) paired in a symmetrical arrangement. The swath widths of these cameras are approximately 413 km and 378 km for the eight off-nadir and nadir ones, respectively. The aerosol properties are retrieved based on the laterally homogeneousness assumption with the $\mathbf{17.6\ km \times 17.6\ km}$ region and minimization of the difference between observed radiances and pre-computed model radiances via the use of a look-up table (LUT). The aerosol model used by the MISR retrieval procedure contains eight different single composition particle types, called components, which are modeled using lognormal size distributions. All components other than dust are assumed to be spherical for the convenient use of the Mie theory to compute the scattering properties. The discrete dipole approximation and the T-matrix technique are used instead for dust components. Combinations of the eight components form 74 distinct mixtures, and thus 74 aerosol models, to simulate the aerosol compositions in the troposphere.

3.4 OMI AAI

The daily Level 3 global gridded absorbing aerosol index (AAI) product that derived from the Aura/Ozone Monitoring Instrument (OMI) onboard the NASA EOS Aura spacecraft are also used to distinguish absorbing aerosol types like biomass burning and dust from non-absorbing aerosols (e.g., sea-salt particles, or sulfates). The measurement of the Earth reflectance by OMI is in the visible and the ultraviolet spectral bands around the globe. Distinguishing absorbing aerosols from non-absorbing ones is based on their spectral contrast in the near-UV region, where ozone absorption is very small. For instance, the absorbing aerosol tends to have large positive AAI, while the non-absorbing aerosol shows near-zero or negative AAI. More details about the near-UV aerosol index retrieval algorithm are described in Torres et al. [37]. The product has a spatial resolution varying

from $\mathbf{13\ km} \times \mathbf{24\ km}$ at nadir to $\mathbf{28\ km} \times \mathbf{150\ km}$ along the scanning edges and it has been available since 2005. We only use data from 2005-2007 for a comparison purpose. However, because of no technique is available to differentiate dust from biomass burning based on solely AAI, this product is just used as an auxiliary tool to characterize the spatial distribution of absorbing aerosols in the first section of our results.

3.5 CALIPSO Data

The CALIPSO data have been available since 2006, as the CALIPO has been launched on 28 April along with the CALIPSO Sun-synchronous satellite in the A-Train constellation. The instrument operates at the dual wavelength (532 and 1064 nm) with the altitude of 702 km during both day and night of the satellite orbit. Three products from the CALISPO are utilized in present study: vertical feature mask (version 3.0.1 and 3.02 level 2), AOD, and the total backscatter coefficient at 532 nm. The former product provides a feature classification between aerosols and clouds, with the spatial resolution varying with respect to the altitude and from horizontal to vertical directions. Horizontally, the spatial resolution are $\mathbf{333\ m}$, 1 km, and 5 km for three atmospheric layers, ground to $\mathbf{8.2\ km}$, $\mathbf{8.2 - 20.2\ km}$, and $\mathbf{20.2 - 30.1\ km}$, respectively. In contrast, the product has much higher vertical resolutions: up to 30 m, 60 m, and 180 m in the three layers, respectively. The CALIPSO vertical feature mask is able to distinguish six types of aerosols (e.g., dust, polluted dust, smoke, etc.) from clouds using a set of algorithms (the cloud-aerosol discrimination algorithm), based on five-dimensional probability distribution functions of the mean attenuated backscatter coefficient at 532 nm, volume color ratio, depolarization, latitude, and layer-center height.

The CALIPSO detects dust aerosols using the volume depolarization ratio (the perpendicular to parallel component of received lidar signals) at 532 nm with a threshold value of 0.6 [24]. All normally defined dust events by horizontal visibility would be likely detected using this threshold value since it corresponds to the dust occurrence with a horizontal visibility exceeding 30 km and a particulate depolarization ratio of 0.35 and a lidar ratio of 45 sr [23]. However, this is not true with 100% credit. Firstly, the current CAD algorithm can still misclassify some dense dust layers as cirrus cloud when they present at high altitudes and/or high latitudes, though it has been improved significantly compared to earlier versions. However, this issue is not a problem because, firstly, Central Asia doesn't situate at high latitude. This paper is to identify the dust aerosol feature based on the feature type along with the quality assurance. We just keep the “dust” and “polluted dust” feature, but consider all other aerosol features (e.g., “smoke”) that we are not interested in as “others”. Because for a very few episodes in Central Asia dust is mixing with other aerosols, disregarding other dust-like features would not yield significant errors.

4. Methodology

The level 2, collection 6 aerosol products from the MODIS contain a parameter, angstrom exponent, which is inversely related to the particle size in general, ranging from $-\mathbf{0.5}$ to $\mathbf{0.5}$ in dusty environment and higher in polluted regions [38]. Dust aerosols (the effective radius in coarse mode: $\sim\mathbf{2\ \mu m}$) are much larger than smoke in size. Thus, the angstrom exponent could be used to distinguish dust particles from aerosols like smoke and urban pollution. Schepanski et al. [39] used 0.6 (the threshold value and hereafter refer as AEt) to screen out fine-mode particles (aged dust, some anthropogenic dust and other types of aerosols in small size), but Ginoux et al. [38] employed a much smaller value, 0 as the threshold. In a recent publication, Xu [40] sets the threshold to be a moderate value, 0.6. For Central Asia, no previous studies are available as our reference. Therefore, a series of AEt values (0.5, 0.7, and 1.0) are used to make conclusions more robust, following Ciren et al. [41]. We refer $\mathbf{AEt} = \mathbf{0.5}$ and 0.7 as the criterion 1 and 2, respectively. The value 1.0 is the largest AEt found in the publication [41] to our best knowledge to screen out fine-mode aerosols together with a second condition of $\mathbf{AOD} > \mathbf{0.2}$. We refer this method as the criterion 3. $\mathbf{AEt} = \mathbf{1.2}$ is also utilized in this study to show influence of the threshold selection on the spatial-temporal variability of derived

Preprints (www.preprints.org) | NOT PEER-REVIEWED | Posted: 11 June 2018 doi:10.20944/preprints201806.0158.v1

Peer-reviewed version available at Atmosphere 2018, 9, 288; doi:10.3390/atmos9080288

dust aerosol optical depth (DOD hereafter) and dust occurrences. Mineral dust is one of the dominant aerosols with a non-spherical shape near desert regions. So, MISR AOD with the non-spherical shape is regarded as dust aerosols in this region.

Figure 2 shows the seasonal mean AOD from Terra, Aqua, SeaWiFS, and MISR of the period 2003-2007 based on which the dust aerosols are obtained. Pixels with all quality flags are used from Terra and Aqua. The analysis period for SeaWiFS and Terra is 2000 to 2010 and 2000 to 2016, respectively. For MISR and MODIS onboard Aqua, it starts from 2003 to 2016. All satellites agree well on the air pollution over the dust source regions surrounding the Aral Sea basin. It is evident that Terra and Aqua show larger seasonal-mean AOD over the Taklimakan Desert in the spring and summer periods. The best estimation for dust AOD is also utilized with quality flags of 2 or 3. MODIS onboard Aqua and Terra has a similar sampling rate, much larger than SeaWiFS and MISR do. Particularly, the pixel amounts for MISR is smaller than for other satellites by approximately an order of 2 due to its narrow swath width. Retrievals are rarely available over the water mask like the Caspian Sea and the Aral Sea (Figure 3).

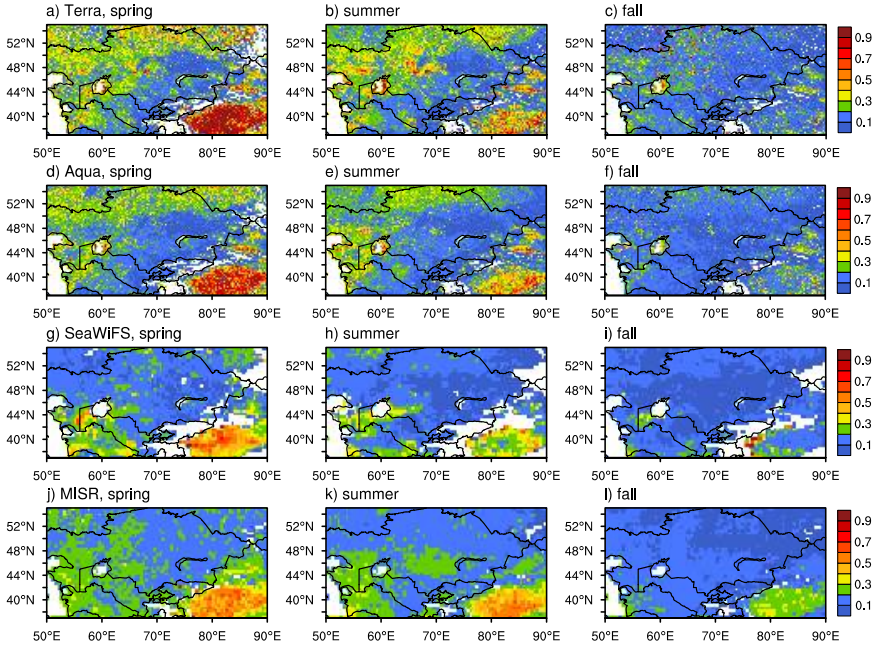

Figure 2. Seasonal distribution of AOD (unitless) from MODIS onboard the Terra and Aqua satellites, SeaWiFS, and from MISR for MAM, JJA, and SON of the 2003-2007 period.

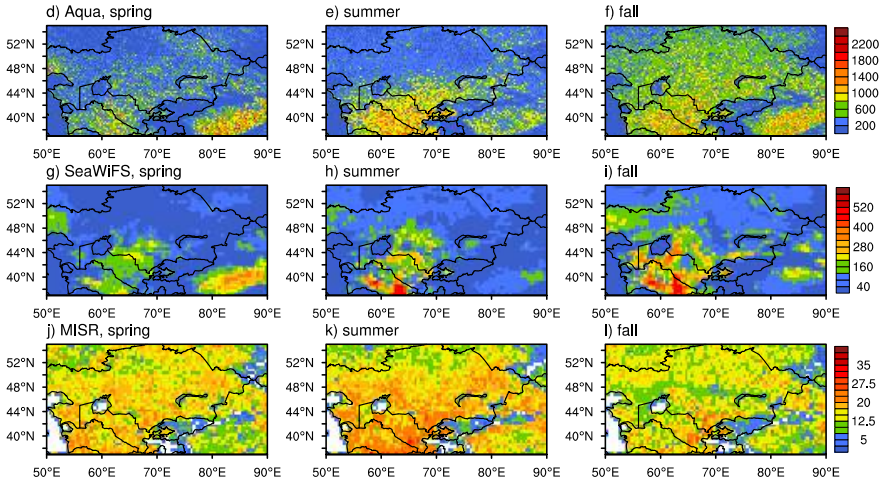

Figure 3. Seasonal mean sampling numbers across Central Asia during the 2003-2007 period.

5. Results

5.1. The Variability of DOD

5.1.1. Spatial Distributions

Figure 4 shows the mean DOD at the 0.55 μm band from the MISR, SeaWiFS, and MODIS onboard Terra and Aqua for spring, summer, and fall seasons of the same period 2003-2007. Despite obviously different coverage areas of DOD>0.3 with respect to seasons, most sensors show high DOD (>0.5) over the Taklimakan Desert, the Ustyurt Plateau, western Turkmenistan, and the Turan Lowland. Only MODIS onboard Terra provides very high DOD (>0.7) over central and western Kazakhstan and the Aral Sea Basin. No retrievals are available from SeaWiFS and MISR over the latter region, as the land algorithms masked out the water pixels. Because of the complex topography, a very limited number of retrievals are made over land patches surrounding Tajikistan and Kyrgyzstan. Available data show very small DOD (<0.2) in this area during the considered three seasons. In the spring and summer, the seasonal mean DOD from Terra is higher than from Aqua and both are higher than from SeaWiFS and MISR, in particular over the Taklimakan Desert. It is very likely that MISR greatly underestimated DOD over the Taklimakan Desert, the Ustyurt Plateau, eastern Kara Kum Desert near the boundary of Turkmenistan and Uzbekistan. In the fall, however, MISR shows higher DOD over the central part of the Taklimakan Desert.

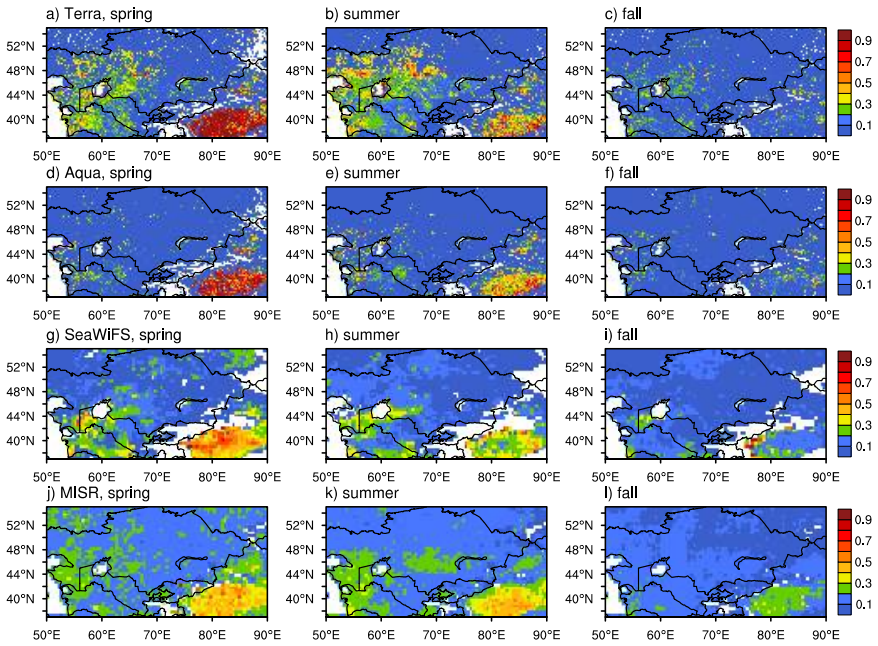

Figure 4. Seasonal mean of DOD in the spring, summer, and fall during the 2003-2007 period from MODIS onboard Terra/Aqua, SeaWiFS, and MISR. White indicates no retrievals available.

In comparison to satellite DOD, the seasonal mean AAI from OMI shows five significant high centers over the Taklimakan Desert, southeast of the Bekdash, the Aral Sea Basin, Urumqi in China, and the Balkhash Lake in decreasing order, as shown in Figure 5. Locations of these centers and areas with AAI higher than 1.2 change only a little bit among the three seasons. The spatial distribution of AI is very similar to the one that obtained by Indoitu et al. [6], although a different period is considered here. As indicated by the shading area with AI greater than 1, dust particles originating from the Aral Kum Desert could be transported hundreds of kilometers away to the east, which is also consistent to their findings. Large patches with high AI (>1.0) can be found in Turkmenistan,

Preprints (www.preprints.org) | NOT PEER-REVIEWED | Posted: 11 June 2018 doi:10.20944/preprints201806.0158.v1

Peer-reviewed version available at Atmosphere 2018, 9, 288; doi:10.3390/atmos9080288

306 western Uzbekistan, southwestern Kazakhstan, and western China, surrounding the high-AI centers.
307 The eastern Kara Kum Desert is not that active as suggested by the derived DOD from MODIS and
308 SeaWiFS, very likely due to a smaller vertical extension of dust plumes in this area.

309 As shown in Figure 4, generally, the seasonal variation of DOD over the western deserts is much
310 smaller than over the Taklimakan Desert, but for some hot spots like the eastern Aral Sea basin they
311 are persistently active through all three seasons with DOD around 0.6. These aspects are also
312 supported by seasonal mean OMI AAI (Figure 5), which identifies much smaller aerosol loading in
313 western Central Asia than in the Taklimakan Desert and similar hot spots with AAI over this basin
314 consistently over 1.0. The seasonal variation of OMI AAI, however, is not as obvious as it is suggested
315 by MODIS-derived DOD, particularly over the western Central Asia deserts. This likely provides the
316 evidence that OMI AAI is insensitive to absorbing aerosols in the low-level atmosphere within the
317 boundary layer, which is typically around 2-3 km in this region (details in the vertical dust plume
318 extension will be discussed in the later section). The small variation, thus, indicates either that most
319 dust particles associated with dust storms present within the low-level atmosphere in the spring or
320 that more present above the boundary layer in the summer and fall such that the OMI can readily
321 capture them. Further study on the vertical structure of dust plumes with respect to seasons is needed
322 to find out the reason of causing the invariant in OMI AAI.

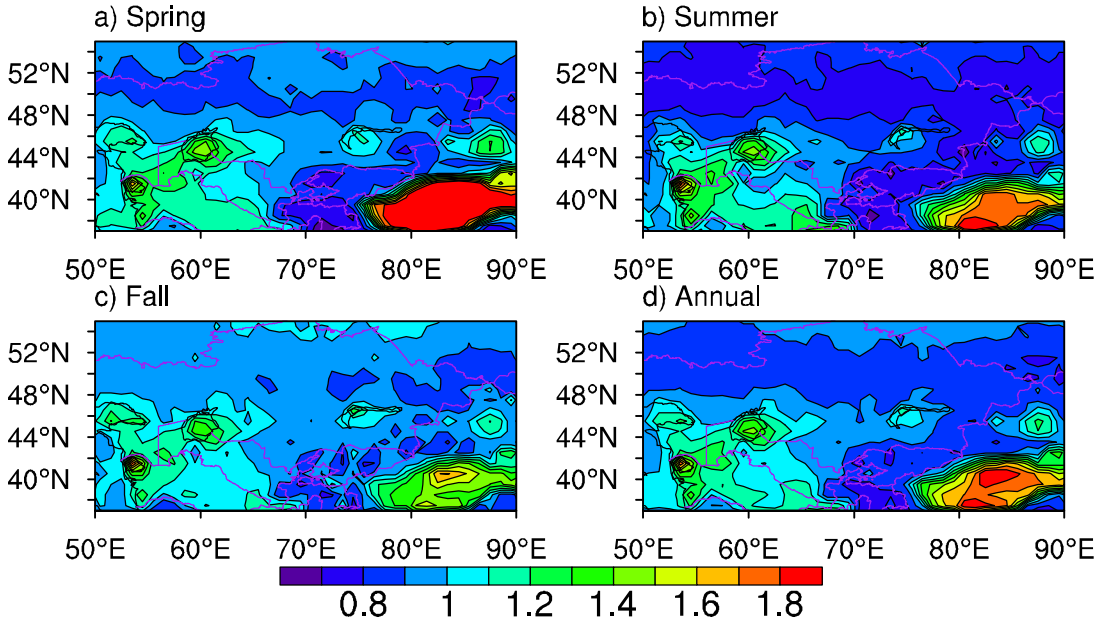

323

324 **Figure 5.** Seasonal mean of AAI for 2003-2007. Panel a), b), c), and d) are for the spring, summer, fall,
325 and the averaging of these three seasons, respectively.

326 5.1.2. The Inter-annual Variability

327 Figure 6 shows the interannual variability of AOD and DOD that obtained with three criterions
328 over the western part of Central Asia from Terra, Aqua, SeaWiFS, and MISR. AOD from different
329 satellites agree very well in terms of annual variability, which is significant during the research
330 period. AOD is limited within 0.1-0.4. High AOD was registered in 2001, 2003, 2007 and it
331 continued until 2014. Extremely high AODs are found in 2009 and 2011, which are evidently greater
332 than in any other years during the research period. AOD with quality flags equal to 2 or 3 is seen
333 smaller than with all flags for both Aqua and Terra satellites except in some years like 2009.

Peer-reviewed version available at Atmosphere 2018, 9, 288; doi:10.3390/atmos9080288

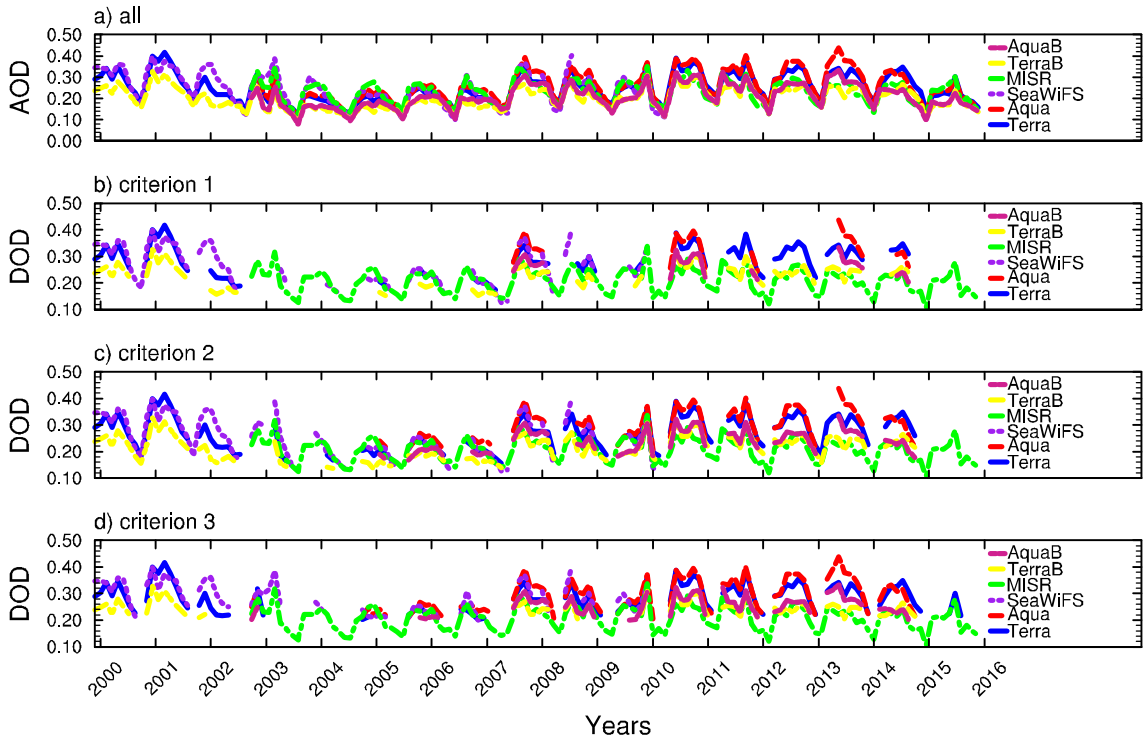

Figure 6. Interannual variability of AOD (a) and dust AOD with the three criterions (b, c, and d) given in Table 1 for the 2000-2016 (Terra), 2003-2016 (MISR), and 2000-2010 (SeaWiFS) periods over the Western Central Asia. TerraB and AquaB represent best estimate with quality flags=2 or 3.

It can be noted that criterion 1 is the most stringent in deriving DOD. Only a small fraction of dust episodes are kept in comparison to the others. According to this criterion and nonzero DOD in at least two satellites retrievals, most dust events occurred during 2000, 2001, 2007, 2008, 2009, 2010, 2011, 2012, 2013, and 2014. It is greatly possible that 2009, 2011, and 2013 are three years that had very intensive dust storms occurred. In fact, based on the measurement taken by Groll et al. [10], the most severe dust storm was registered in September 2009 in Uzbekistan due to very strong surface winds. Limited information is further available on that dust storm case. In contract, another extreme dust storm that has been well studied [42] was registered in April of 2001, lasting for several days after the maximum emission date on April 8. This event can also be seen in DOD from MODIS onboard the Aqua and Terra satellite. The dry condition and strong surface winds over the dust source regions, Aral Sea basin, the Ustyurt Plateau etc., induced intensive dust emissions. During 2002, 2003, and 2004, very few dust events occurred in general. So, the AOD remained low and DOD became zero.

In contract to the western part of Central Asia, the DOD amplitudes exhibit a significant difference among the four sensors over the Taklimakan Desert (Figure 7). The annual variability of DOD is again similar among the four sensors, but MODIS tends to show higher amplitude than the others do. AOD from Aqua and Terra are perfectly overlapping with each other no matter whether restrictions are placed on pixels according to their quality flags. Dust events are more frequent and intensive in general over the Taklimakan Desert than over the western part of Central Asia. Because aerosols in this region are far dominant by mineral dust, applying different Angstrom exponent thresholds has negligible influence on the annual variability of DOD.

Preprints (www.preprints.org) | NOT PEER-REVIEWED | Posted: 11 June 2018 doi:10.20944/preprints201806.0158.v1

Peer-reviewed version available at Atmosphere 2018, 9, 288; doi:10.3390/atmos9080288

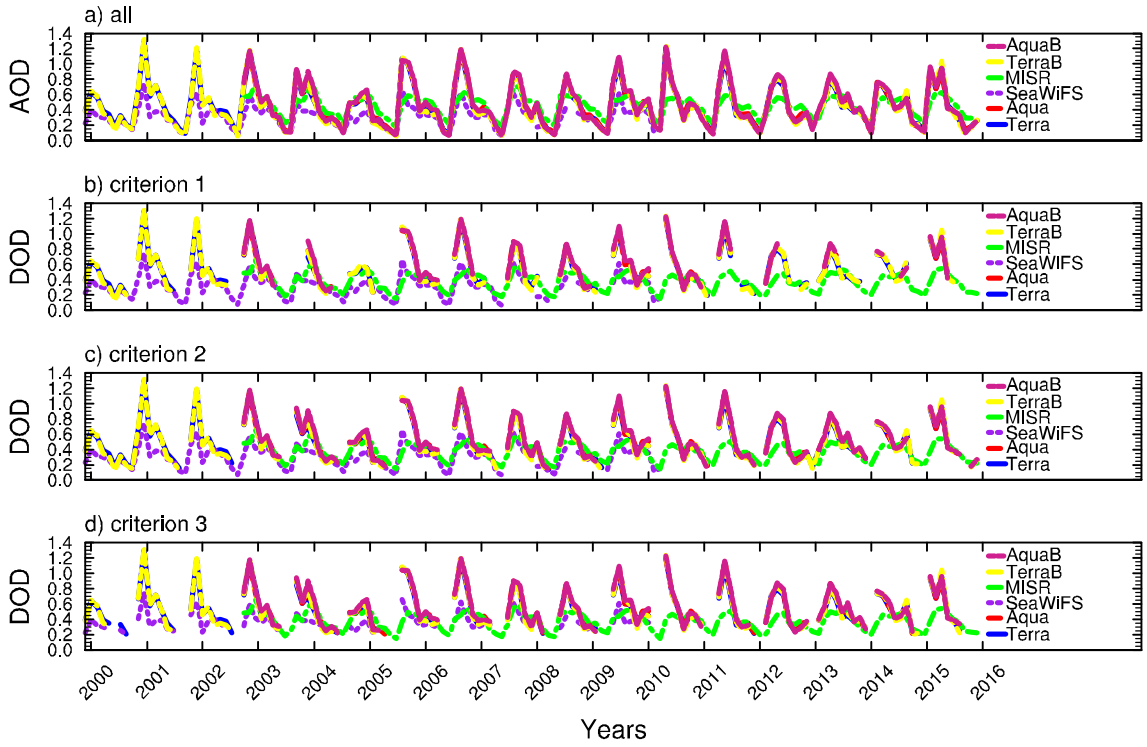

Figure 7. Same as Figure 6, but for the Taklimakan Desert.

A comparison of AOD and DOD among Aqua, SeaWiFS, MISR, and Terra is done on the daily and monthly basis over the western part of Central Asia and the Taklimakan desert, as illustrated in Figure 6, 7. Over the Taklimakan Desert, Aqua AOD is very close to that from Terra, but AODs from MISR and SeaWiFS are evidently smaller than from Terra and Aqua on both daily and monthly basis. Over the western Central Asia, it is a little bit smaller than the latter one. These statements well apply to both AOD and DOD with all the three criterions. In terms of daily AOD/DOD with all quality flags and the best estimation, Aqua is comparable to Terra over the western part of Central Asia. However, the best estimated AOD/DOD from SeaWiFS is larger than from Terra on monthly basis, but the former becomes smaller, if all quality flags are applied. DOD derived from the MISR is smaller than from any other satellites over the western part of Central Asia (the Taklimakan Desert) on monthly (daily) basis.

5.1.3. The Seasonal Variability

Figure 8 presents the annual distribution of the monthly mean AOD and DOD statistic metrics (minimum, maximum, median, and 5% and 95% quintiles) over the Taklimakan Desert. The associated periods are 2000-2016, 2003-2016, and 2000-2010 for MODIS onboard Terra/Aqua, SeaWiFS, and MISR, respectively. Consistent to the mean values, AOD and DOD from SeaWiFS and MISR are systematically smaller than from MODIS onboard Terra and Aqua in all statistic parameters. Both MODIS and SeaWiFS identify the spring as a season with the highest AOD/DOD, but MISR doesn't provide a clear seasonal variation with AOD/DOD only slightly higher in May (median: 0.53) than in other months, whatever criterion is utilized. The smallest DOD is seen in October, but the smallest AOD is in November. The month November tends to have more extreme cases with the AOD significantly exceeding the statistic metrics from MODIS aerosol products. With criterions applied to AOD, one can find these extreme cases are absent from the MODIS-derived DOD, yielding a higher value in this month than in October. Similar results could be seen over the western part of Central Asia, but the seasonal variability is not as obvious as over the Taklimakan Desert.

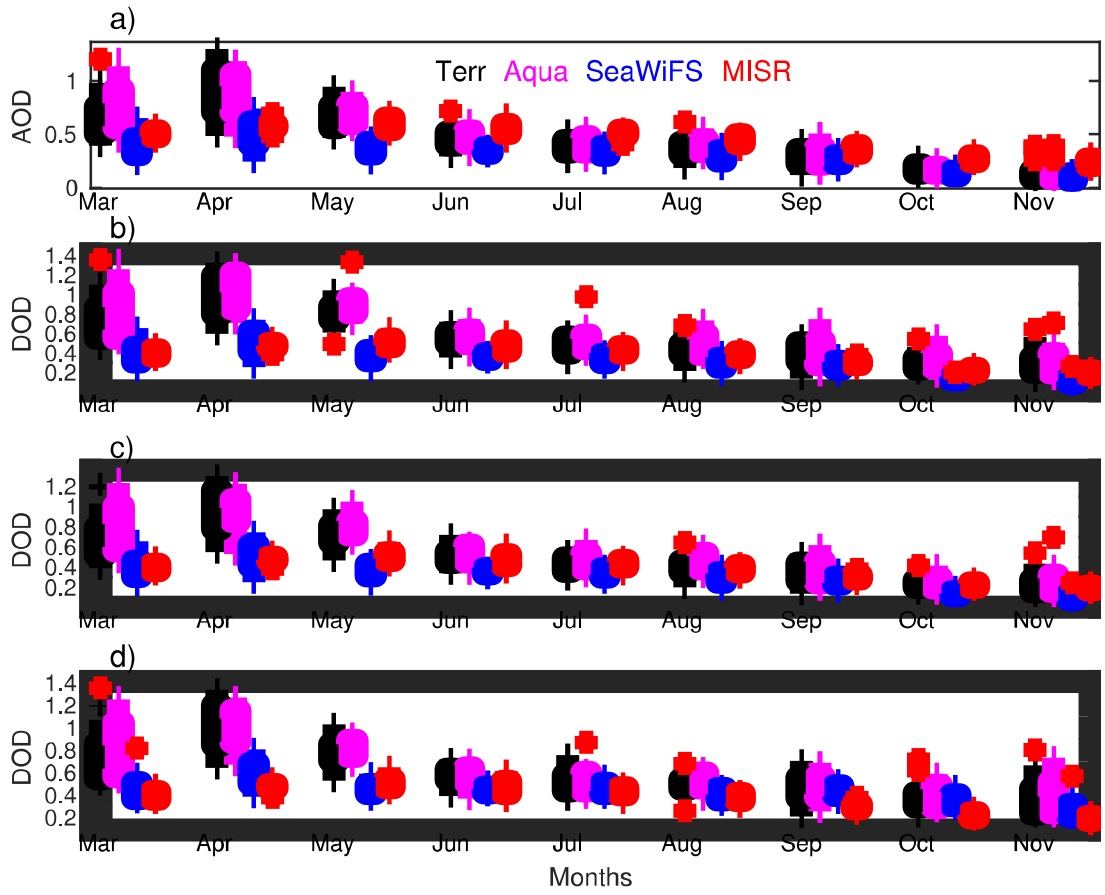

Figure 8. The statistic metrics of the annual distribution of monthly mean AOD (a) and derived DOD (0.55 μm) with the three criterions (b, c, and d corresponding to Criterion 1, 2, and 3, respectively) during the examined period from MODIS, SeaWiFS, and MISR. The red "+" indicates AOD/DOD of extreme cases.

The amount of invalid satellite sampling pixels is not homogenously among the three seasons, which could bias the results obtained from simple mean or median values. For instance, much less frequent AOD retrievals are available in the winter due to ice- or snow-covering and in the spring (Figure 3, d, g) because of a higher frequency of cloud appearances in comparison to the other seasons. For Central Asia, as the winter is already excluded, the problem doesn't reside in the ice- or snow-covering, but after applying a threshold to the satellite data such that non-dust aerosols are efficiently excluded, the heterogeneous amount of valid AOD/DOD points still exist among three seasons. To overcome this issue, we applied the one-sided Wilcoxon sum rank test on the null hypothesis of equal median distributions to robustly explore whether there is a statistically significant seasonal variation in the satellite-derived DOD with the best estimation quality flag, as shown in Table 1. Generally, most tests with four different sensors confirm the significantly higher DOD in the spring (MAM) than in the summer (JJA) or fall (SON) at a confidence level of 99% over the Taklimakan Desert and the western Central Asia. This holds, as whatever threshold values have been selected to remove non-dust particles like smoke, sea salt, etc, demonstrating that the higher dust amount in the spring is a robust conclusion that presents in the satellite data, as all p-values are very close to zero. Two exceptions are tests that constructed on the equality between the spring and summer seasons over the western Central Asia using criterion 3 based on Terra (p-value=0.55), Aqua (p-value=0.096), and SeaWiFS (p-value=0.0915). Not enough evidence exists to conclude that higher DOD appears in the former season at the 99% test level. As indicated by p-value=0.001 and 0.00000231, higher AOD is found in the summer rather than in the spring by MODIS onboard both Terra and Aqua, contrary to conclusions by the other sensors.

Preprints (www.preprints.org) | NOT PEER-REVIEWED | Posted: 11 June 2018 doi:10.20944/preprints201806.0158.v1

Peer-reviewed version available at Atmosphere 2018, 9, 288; doi:10.3390/atmos9080288

Table 1. P-values from the Wilcoxon sum rank test on AOD and DOD that derived using the three criterions, criterion 1, criterion 2, and criterion 3, for the seasonal variation over the western Central Asia (Cen) and the Taklimakan Desert (Tak). The test is made using AOD/DOD with the quality flag =2 or 3; The upscript 1 shows test between MAM and JJA, rather than JJA and MAM (Note the order matters in the Wilcoxon sum rank test).

P-Values	**Regions**	**Sensor**							
		Terra		Aqua		SeaWiFS		MISR	
		JJA vs MAM	SON vs MAM	JJA vs MAM	SON vs MAM	JJA vs MAM	SON vs MAM	JJA vs MAM	SON vs MAM
AOD	Cen	2.10(-1)	4.06(-90)	3.65(-02)[1]	4.74(-97)	2.14(-07)	3.16(-155)	5.38(-05)	4.35(-137)
	Tak	3.65(-94)	1.19(-258)	1.49(-77)	2.56(-227)	1.33(-10)	1.43(-126)	1.18(-09)	6.52(-143)
Criterion 1	Cen	1.57(-15)	2.02(-26)	5.48(-06)	2.42(-21)	4.55(-10)	1.05(-73)	4.14(-02)	7.10(-104)
	Tak	2.43(-80)	7.15(-83)	1.43(-53)	1.04(-60)	8.09(-10)	5.50(-96)	2.77(-04)	7.39(-123)
Criterion 2	Cen	2.31(-10)	8.47(-45)	9.78(-05)	6.29(-37)	3.15(-12)	1.90(-104)	4.14(-02)	7.10(-104)
	Tak	5.56(-83)	9.35(-128)	1.26(-66)	7.48(-98)	4.57(-10)	3.62(-108)	2.77(-04)	7.39(-123)
Criterion 3	Cen	4.80(-03)	2.10(-20)	7.30(-03)	1.48(-16)	2.41(-05)	6.28(-23)	4.14(-02)	7.10(-104)
	Tak	1.38(-38)	4.43(-37)	1.81(-30)	1.36(-33)	1.58(-04)	2.80(-07)	2.77(-04)	7.39(-123)

5.2. Dust Occurrences

It is useful to derive the dust occurrence in addition to presenting AOD and DOD, firstly for a comparison purpose, since most existing publications are addressing the dust events using the frequency, secondly for the monitoring purpose, and, finally, because of its severe consequence on the air quality near the source areas. Therefore, based on the dust climatology dataset presented in previous section, we calculate the dust event numbers in this section by applying a threshold constant to MODIS DOD (referred to DODt hereafter). Note if DOD at a location on a day exceeds the given DODt, we define it as a dust event. MISR-derived and SeaWiFS-derived DOD are not further utilized in this section, because of the limited amount of retrievals and much smaller values and variance in comparison to MODIS-derived one, as found above (Figure 7 and Figure 8). AOD retrievals with all quality flags are used here following the recommendation by Baddock et al. [43] to derive the dust occurrence numbers, because the quality flag is not well marked over desert regions where a larger standard deviation is always found [4]. Consistent to Baddock et al. [43], a threshold DODt=0.2 is also applied in the present study to count the dust occurrence numbers. To avoid the contamination of the use of a threshold constant on the results, a series of threshold values close to 0.2 will be applied to the dust event selecting procedure to yield a more robust conclusion.

5.2.1. Spatial Distributions

Figure 9 shows the calculated dust occurrence numbers based on the threshold value of 0.2 using DOD by MODIS onboard Terra during 2000-2016. Obviously, the spatial distribution of the calculated dust occurrence numbers is similar to that of high DOD (>0.2, Figure 4 a, b, and c) and AI (>1.0, Figure 5). Persistently active dust activities can be seen over the Taklimakan Desert, the Aral Kum Desert, the Ustyurt Plateau, and the western Turkmenistan. The use of different AEt values to remove non-dust aerosols doesn't change the calculated dust occurrence numbers a lot, particularly over the Taklimakan Desert, where the least sensitivity of the spatial coverage of dust occurrences numbers to AEt is found. An increase of the angstrom exponent from 1.2 to 2.0 only leads to a slight expansion of the horizontal distribution, pushing the area with the dust occurrence numbers greater than 80 days northward into the northern Kazakhstan.

Preprints (www.preprints.org) | NOT PEER-REVIEWED | Posted: 11 June 2018 doi:10.20944/preprints201806.0158.v1

Peer-reviewed version available at Atmosphere 2018, 9, 288; doi:10.3390/atmos9080288

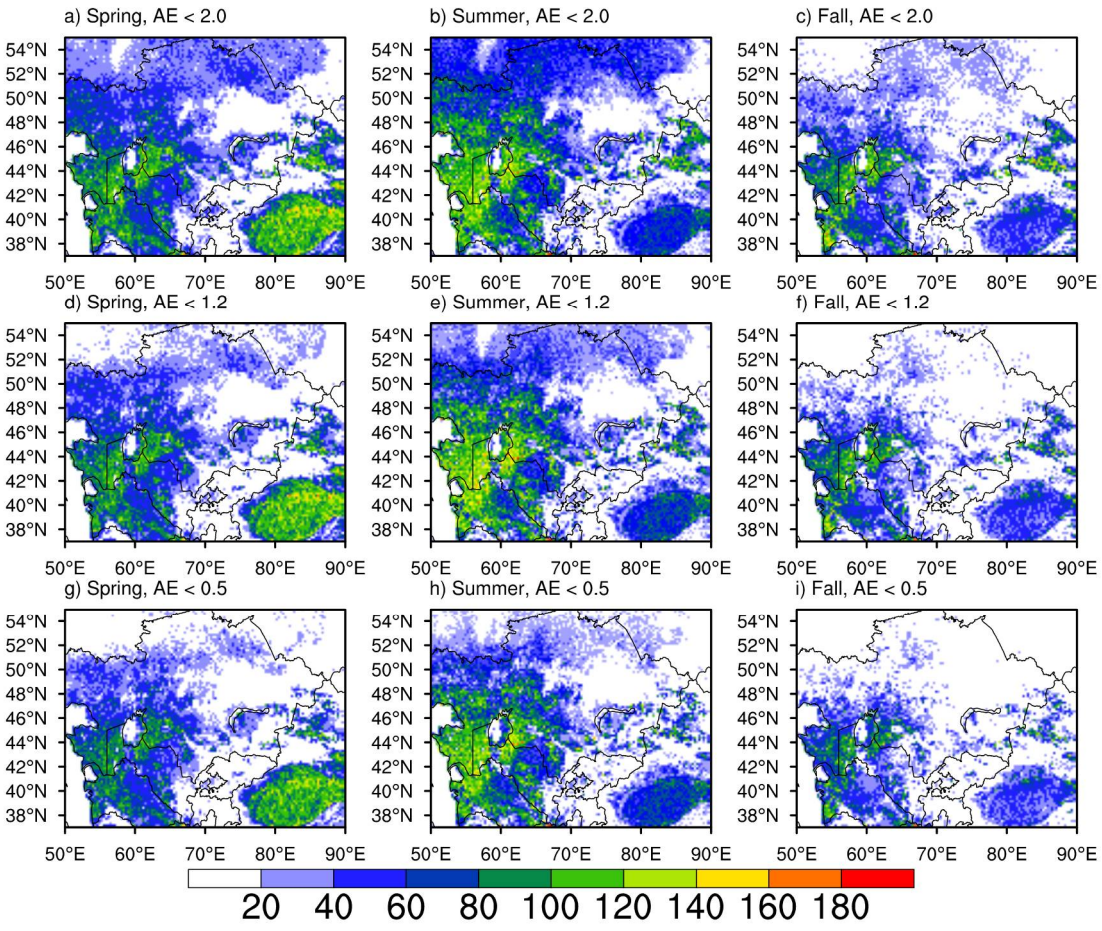

Figure 9. Spatial distributions of the dust occurrence number during the 2000-2016 period in the spring (a, d, and g), summer (b, e, and h), and fall (c, f, and i) seasons with different Angstrom exponents as the threshold: AEt=2.0 for a, b, and c; AEt=1.2 for d, e, and f; AEt=0.5 for g, h, and i.

Numbers of the dust occurrence for four sub-regions stratified by four AEt and three DODt values are summarized in Table 2. The least sensitivity of the sub-domain averaged dust occurrence number to both AEt and DODt can be seen over that of the Taklimakan Desert while the largest one is over the Aral Kum Desert. For DODt=0.2, the use of AEt=2.0 in comparison to that of 0.5 leads to an increase of the dust occurrence number by approximately 21, 15, and 24 in the spring, summer, and fall, respectively, with the relative percentage slightly larger than 20% over the latter area (the Aral Kum Desert) in contrast to 7, 5, and 11 over the former Desert. However, if a lower DODt is used, e.g., 0.1, the dust occurrence number raise up rapidly from 47, 66, and 29 to 96, 141, and 95 in the spring, summer, and fall, respectively, in comparison to the case of DODt=0.3, indicating a higher sensitivity of the calculated dust occurrence number to DODt than to AEt over the Aral Kum Desert. Similar results can also be seen in other locations. Although the dust occurrence number could change a lot, if different DODt or/and AEt are applied to the calculation given a fixed location, its rank among the four sub-regions remains unchanged in a specific season. For instance, highest value is found over the Taklimakan in the spring (78-114 days) and over the Ustyurt Plateau in the summer (93-166). It seems that, even though AOD and/or DOD are both smaller, the Ustyurt Plateau has been experiencing a more frequent dust occurrence than the Taklimakan Desert. It continues active through all the three seasons during the study period (2000-2016), as can be intuitively seen in Figure 9.

Table 2. Dust occurrence numbers for four sub-regions (Kaza: Kazandzhik; Usty: Ustyurt Plateau; Takl: Taklimakan; Aral: Aral Kum), as labeled by the purple boxes in Figure 1, with three different DOD thresholds (0.1, 0.2, and 0.3) and four Angstrom exponent thresholds (2.0, 1.2, 0.7 and 0.5). The

last two Angstrom exponent thresholds correspond to Criterion 2 and Criterion 1, respectively. All quality levels from MODIS/Terra are used. Note numbers in parenthesis of the first three columns represent relative percentages (%) between dust occurrence numbers with AEt=0.2 and those with AEt=0.5. Similarly, numbers in square brackets represent relative percentages (%) between dust occurrence numbers with DODt=0.1 and those with DODt=0.3 for AEt=0.7.

		AE<2.0			AE<1.2			AE<0.7			AE<0.5		
DOD>	regions	Spring	Summer	Fall	Spring	Summer	Fall	Spring	Summer	Fall	Spring	Summer	Fall
	Kaza	104(20)	153(15)	129(29)	95	143	112	90[84]	136[77]	104[148]	87	133	100
0.1	Usty	107(22)	166(13)	122(24)	97	157	107	91[52]	150[58]	100[138]	88	147	98
	Takl	114(9)	87(6)	72(16)	112	85	68	107[35]	82[71]	63[152]	105	82	62
	Aral	116(25)	159(15)	123(35)	103	148	103	96[104]	141[114]	95[228]	93	138	91
	Kaza	80(18)	120(14)	87(23)	75	114	80	71	108	74	68	105	71
0.2	Usty	89(17)	138(11)	81(16)	83	132	77	78	127	72	76	124	70
	Takl	95(7)	64(5)	42(11)	94	64	41	91	62	38	89	61	38
	Aral	86(21)	116(15)	72(24)	80	110	66	74	104	61	71	101	58
	Kaza	55(17)	86(15)	49(23)	52	81	46	49	77	42	47	75	40
0.3	Usty	66(14)	103(11)	47(15)	63	99	45	60	95	42	58	93	41
	Takl	83(6)	49(4)	27(13)	82	49	26	79	48	25	78	47	24
	Aral	55(22)	75(17)	34(21)	51	71	32	47	66	29	45	64	28

5.2.2. The Inter-annual Variability

According to Section 5.2.1., the dust occurrence number is monotonically increasing with respect to AEt at a slower rate than with respect to DODt. Therefore, calculations of this part are made on three DODt values (0.1, 0.2, and 0.3) and two AEt values (1.2 and 0.5) only. Figure 10 shows the interannual variability of the dust occurrence calculated over the four sub-regions as labeled in Figure 1 during 2000-2016. The interannual variability of dust occurrences that are derived using different DODt and AEt values is consistent among the four sub-regions, but some differences are distinct between the Taklimakan Desert and the other three sub-regions. The Taklimakan Desert has a lower dust occurrence and year-to-year variation than the others during the research period. We found the dust occurrence is decreasing from 2013 to 2014 over the Taklimakan Desert, but it is increasing over the other three sub-regions. High dust occurrences are found in 2006, 2009, and 2010, which is consistent to the finding by Groll et al. [10], based on the ground measurement on dust depositions in Central Asia. The effect of using different AEt and DODt values on the dust occurrence calculation also presents an obvious year-to-year variation, but it is consistent to the finding shown in Section 5.2.1. that dust occurrences are more sensitive to AEt than to DODt, in general, particularly over the Taklimakan Desert. AEt has a greater effect over the Kazadzhik, the Ustyurt Plateau, and the Aral Kum Desert for DODt=0.1 than for DODt=0.3, which might provide an evidence of the find-mode dominance in the low AOD case. However, it is unfair to set a low bound when deriving DOD, because theoretically to say dust particles can present for all AOD values.

Preprints (www.preprints.org) | NOT PEER-REVIEWED | Posted: 11 June 2018 doi:10.20944/preprints201806.0158.v1

Peer-reviewed version available at Atmosphere 2018, 9, 288; doi:10.3390/atmos9080288

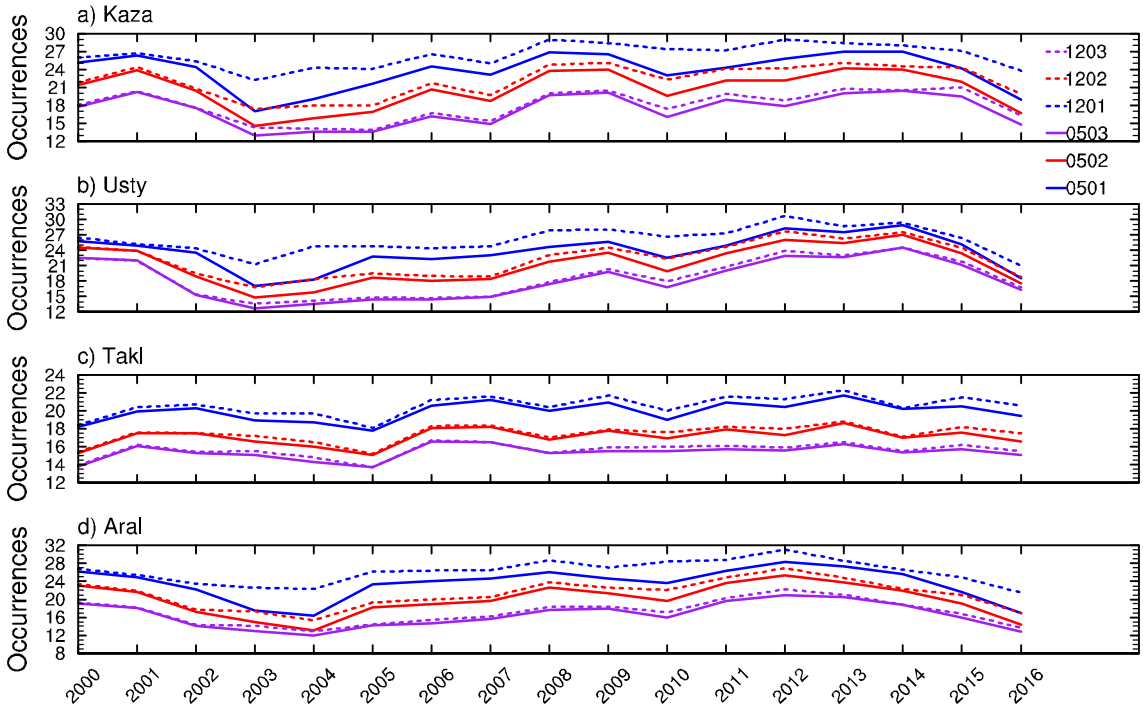

Figure 10. The inter-annual variability of dust occurrences that obtained by applying two AEt and three DODt values to MODIS/Terra AOD over the four sub-regions (a: Kaza-Kazandzhik; b: Usty-Ustyurt Plateau; c: Takl-Taklimakan; d: Aral-Aral Kum) during the 2000-2016 period. The legend labels represent AEt and DODt, for instance, 1203 means AEt=12 and DODt=3.

The trend analysis is also made using a non-parametric statistic method, Mann-Kendall, following Li and Sokolik [4], for the four sub-regions. No assumption on the distribution is required and the outliners have a negligible influence on the test result in this method. Table 3 shows that positive but not statistically significant trends are observed for all targeted regions at a confidence interval of 95%, suggesting a longer time spanning is needed for a more robust result. The largest trend of the dust occurrence during the 2000-2016 period is found over the Ustyurt Plateau approximately 0.22, 0.47, and 0.52 per year for DODt=0.1, 0.2, and 0.3, respectively, using AEt=0.5 according to this method. The positive trend based on DODt=0.3 and AEt=0.5 is not statistically significant at the confidence level of 95%, but it becomes significant at a just smaller confidence level, 90%. The dust occurrence over the Taklimakan stays stable during this period with the trend very close to 0, whatever DODt and/or AEt are utilized. Consistent to previous sections, the trend over the Taklimakan Desert is less sensitive to AEt than over the other sub-regions.

Table 3. Trend (per year) and associated p-values with the confidence interval of 0.95 for dust occurrences derived from MODIS/Terra ADO over the four sub-regions during 2000-2016 by a non-parametric test, Mann-Kendall.

		DODt=0.1		DODt=0.2		DODt=0.3	
	Sub-regions	Trend	P-values	Trend	P-values	Trend	P-Values
AEt=0.5	Kaza	0.0829	0.5098	0.1658	0.2661	0.1679	0.2322
	Usty	0.2325	0.174	0.4725	0.2165	0.5167	0.0581
	Takl	0.0817	0.1175	0.05	0.3031	0.0333	0.3648
	Aral	0.1464	0.5366	0.1958	0.3434	0.1917	0.2322
	Kaza	0.1625	0.2016	0.2045	0.0836	0.2038	0.1082
	Usty	0.2086	0.1082	0.4023	0.174	0.3833	0.0529

Preprints (www.preprints.org) | NOT PEER-REVIEWED | Posted: 11 June 2018 doi:10.20944/preprints201806.0158.v1

Peer-reviewed version available at Atmosphere 2018, 9, 288; doi:10.3390/atmos9080288

AEt=1.2	Takl	0.1225	0.0529	0.069	0.1494	0.0542	0.2487
	Aral	0.1958	0.2322	0.2643	0.2322	0.2367	0.174

514 5.2.3. The Seasonal Variability

515 As can be seen from Figure 9, the area with the dust occurrence numbers exceeding 80 days in
516 total within in each season are mainly found over the Taklimakan Desert during the spring season.
517 In summer and fall seasons, the dust occurrence are both lower than 80 days over the whole desert
518 region. It seems that there also exists a season variation of dust occurrences. We then calculated the
519 median, 5% and 95% quintiles, minimum, and maximum of the dust occurrence that derived from 3
520 DODt for the four sub-regions, as shown in Figure 11.

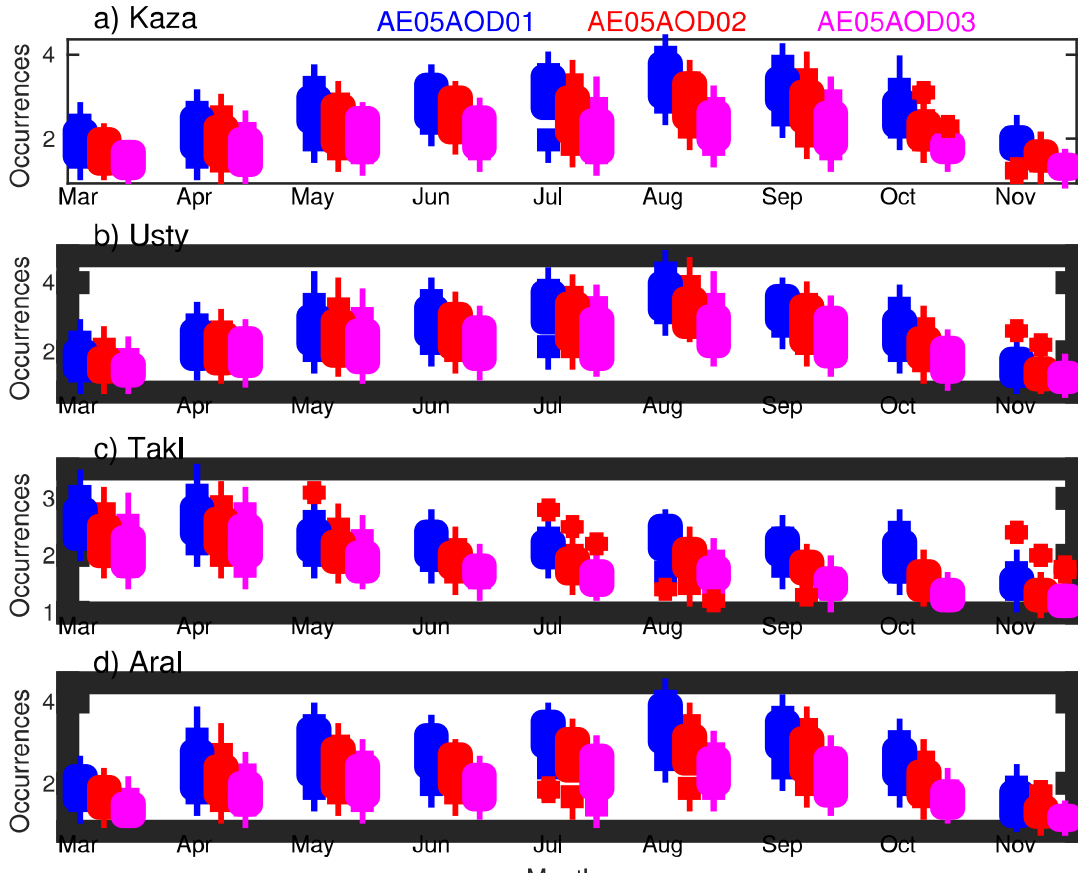

521

522 **Figure 11.** The statistic metrics of the annual distribution of dust occurrences that derived from
523 MODIS/Terra AOD over the four sub-regions (a: Kaza, eastern Turkmenistan; b: Usty, Ustyurt
524 Pleateau; c: Takl, the Taklimakan Desert; d: Aral, the Aral Sea Basin), as labeled in Figure 1, using
525 three DODt (blue: 0.1; red: 0.2, and purple: 0.3). The red "+" indicates AOD/DOD of extreme cases.

526 The one-sided Wilcoxon Sum Rank test is again applied to the derived dust occurrence based
527 on MODIS/Terra AOD such that a robust conclusion could be achieved. The p-values for the four
528 sub-regions are summarized in Table 4 based on 3 DODt and 2 AEt among the paired spring,
529 summer, and fall seasons. For the three sub-regions over the western part of Central Asia all p-values
530 between MAM and JJA are close to 0, indicating the dust occurrence is statistically higher in the
531 summer than in the spring. Similarly, statistically higher dust occurrence in the summer season than
532 in the fall is seen. Comparisons between the spring and fall seasons are distinct over these sub-
533 regions. P-values over the Ustyurt Plateau and the Aral Kum are 0.88 and 0.37, respectively, using
534 DODt=0.1. It is also the case, if different DODt values are used instead. So, no evidence is displayed
535 to support that any significant difference of the dust occurrences between the spring and fall seasons

exists. The seasonal variation of the dust occurrence is more sensitive to AEt than the seasonal variation of AOD/DOD is, because the p-values over the two sub-regions become greater than 0.95, if AEt=1.2 is used. The dust occurrence is higher in the spring than in the fall, according to the p-values (0.0139), over the Kazandzhik, using DODt=0.1, but it becomes insignificant, if a higher DODt is used. Over the Taklimakan Desert, the spring season has the most frequent dust occurrence, followed by the summer and differences among the paired seasons are significant for all thresholds.

Tables 4. P-values from the Wilcoxon sum rank test on the seasonal variation of dust occurrence that derived using several criterions, AEt=0.5 and AEt=1.2 against DODt=0.1, DODt=0.2, and DODt=0.3 over the four subregions as shown by boxes in Figure 1.

		DODt=0.1			DODt=0.2			DODt=0.3		
	regions	MAM vs JJA	MAM vs SON	SON vs JJA	MAM vs JJA	MAM vs SON	SON vs JJA	MAM vs JJA	MAM vs SON	SON vs JJA
	Kaza	2.14(-10)	0.9871	6.09(-05)	1.92(-08)	0.89	1.59(-05)	2.95(-07)	0.61	1.86(-06)
	Usty	3.19(-10)	0.88	4.52(-06)	1.06(-08)	0.53	1.02(-06)	3.97(-07)	0.17	2.79(-07)
AEt=0.5	Takl	3.84(-05)	7.2(-10)	3.82(-04)	1.79(-06)	5.92(-15)	3.76(-08)	5.79(-09)	5.01(-17)	1.07(-10)
	Aral	1.33(-07)	0.37	1.59(-05)	6.78(-06)	0.69	1.97(-05)	1.21(-05)	0.89	1.21(-06)
	Kaza	1.06(-12)	0.999	9.82(-04)	1.22(-09)	0.92	1.6(-05)	7.51(-08)	0.45	5.51(-07)
	Usty	1.06(-11)	0.98	3.6(-05)	2.4(-09)	0.48	6.51(-07)	3.84(-07)	0.063	7.5(-08)
AEt=1.2	Takl	3.97(-06)	2.41(-09)	0.55(-02)	1.51(-07)	3.88(-15)	2.8(-07)	4.19(-10)	3.1(-17)	1.16(-09)
	Aral	6.27(-09)	0.1	4.13(-04)	1.36(-06)	0.77	1.33(-05)	6.58(-06)	0.94	2.71(-07)

5.3. Physical properties and Vertical Profiles of Dust Aerosols

One dust case that occurred on May 7 2007 is chosen here to analyze the dust vertical distribution in Central Asia. A dominant fraction of dust particles was originating from the Aral Kum, according to the model simulation [35]. MODIS onboard the Terra satellite happened to capture this dust storm as well, as the retrieved AOD using the deep blue algorithm reached up to 3.5 to the southern edge of the sea basin. Plots of the subtype features of the CALIPSO VFM indicate a limitation of dust vertical extension for this event within the boundary layer not exceeding 3 km (Figure 12). At the early stage of the storm, the retrieval detected freshly pure mineral dust (Figure 12a) which was transformed to polluted dust (Figure 12b). The different subtypes very likely provide an evidence of aging processes after main dust storms by taking non-mineral aerosols like salt, smoke, hydrogen carbonate. It has a possibility that mineral dust is originally mixing with other compositions like salt, hydrogen carbonate, and sulfate in the soil. But the amount of these non-minerals was experiencing a rapid increase in the dust particles. Razakov and Konsnazarov [44] found that dust deposits close to the Aral Kum desert contains a considerable fraction of sea salts up to 20-30%. The recent chemical analysis[10] with samples taken from stations close to the Aral Kum, however, found a mixing of non-mineral compositions (hydrogen carbonate, sulfate, calcium, chloride). Efforts in quantifying differences between compositions of dust aerosols and those of the source soil are needed to ensure their mixing state and to learn about aging processes of the freshly emitted particles.

Preprints (www.preprints.org) | NOT PEER-REVIEWED | Posted: 11 June 2018 doi:10.20944/preprints201806.0158.v1

Peer-reviewed version available at Atmosphere 2018, 9, 288; doi:10.3390/atmos9080288

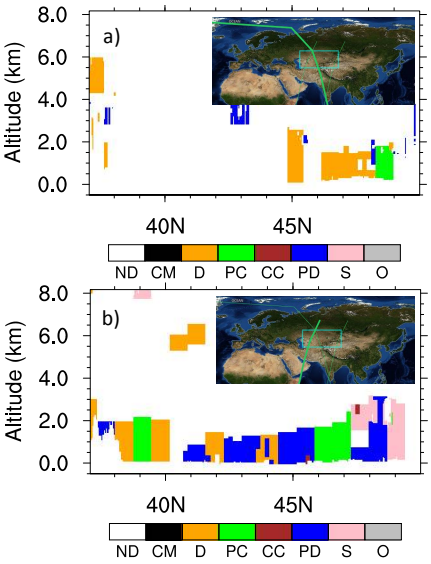

564

565 **Figure 12.** Vertical Feature Mask (VFM) from CALIPSO (left panel during daytime and right panel
566 during nighttime) for a dust storm occurring on May 7 2007 over the Aral Sea Basin. Subplots in both
567 plots show the CALIPSO track, as indicated by green line over Central Asia (the domain is labeled
568 by green boxes). ND: not determined; CM: clean marine; D: dust; PC: polluted continental; CC: clean
569 continental; PD: polluted dust; S: smoke; O: other.

570 The deployment of lidar makes qualitative analysis available on the aerosol extinction coefficient
571 profile, which is one of the most uncertain factors in modeling the radiative process. Based on the
572 vertical feature mask, we selected several dozens of dust events which have been captured by
573 CALIPSO to calculate the mean extinction profile at 532 nm, as shown in Figure 13, along the satellite
574 path covering main dust source regions including the Aral Kum Desert, the Kyzyl Kum Desert, the
575 Ustyurt Plateau, the Kara Kum Desert, and the Taklimakan Desert in 2007. Of the selected dust
576 events, 66 are seen over the western part of Central Asia and 17 over the Taklimakan Desert.
577 Approximately 16.8% are found during the daytime and 38.65 in the summer season. All pixels which
578 have been classified as non-aerosols or/and non-dust aerosols are removed based on the CALIPSO
579 feature and sub-feature types. Note we retained polluted dust, which is classified as a separate
580 subtype from dust by CALIPSO, in the analysis, as it is difficult to distinguish whether the mixing is
581 made in the atmosphere after emissions or originally in the soil. To further control the data quality,
582 we also remove low confident retrievals that have the CAD_score (the cloud-aerosol discrimination
583 score) out of the range from -100 to -20 and the extinction uncertainty exceeding 120%.

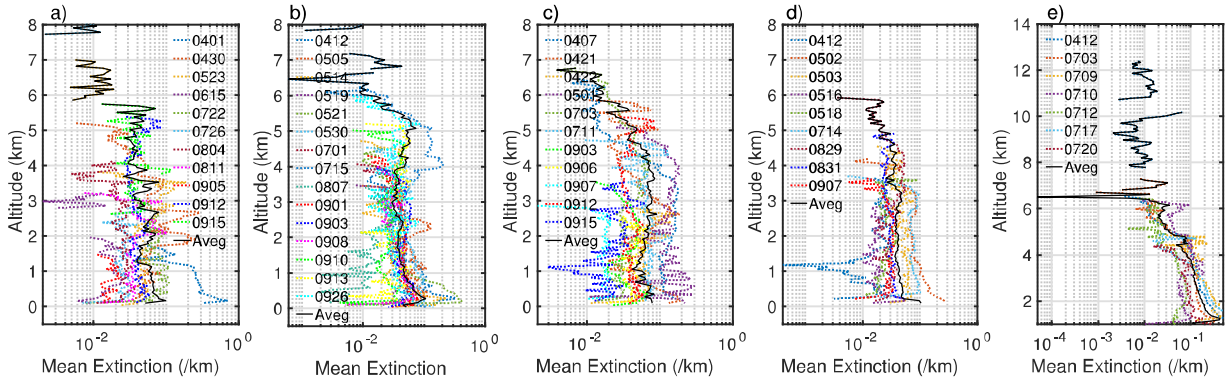

584

585 **Figure 13.** Aerosol extinction coefficient profiles for selected caces with the height above the sea
586 surface level over the following sub-regions: a) the Aral Sea Basin, b) Ustyurt Plateau, c) the Kara
587 Kum Desert, d) the Kyzyl Kum Desert, and e) the Taklimakan Desert.

In general, no evident differences exist among the four sub-regions in the western Central Asia. The Taklimakan Desert has a systematically larger mean extinction and the extinction remains large until the high troposphere. Most dust particles are located at the low-level layer within 2 km away the surface with the extinction decreasing oscilatelly from the surface to the top boundary layer, but the extinction profile spreads a lot from one event to another, particularly over the Kara Kum Desert. The peaking (0.09 km^{-1}) of the extinction profile averaged over these events is seen approximately at 3.6 km, which is quite different from the other source regions where dust plumes peak are very close to the surface. Effective vertical transport can also be seen for some cases via the mean extinction profile, although the maximum value appreas near the surface. For instance on May 1 2017, the mean extinction reaches up to 0.19 km^{-1} around 3.8 km over the central Kara Kum Desert. For the event on April 7, dust aerosols were lifted up effectively to approximately 5.6 km over the Kara Kum Desert. Another evident characteristic of the mean extinction profile for the later event is the multiple structure with another two minor peaks at layers around 2.6 km and 5 km. According to the selected cases, the dust extinction is weaker in September and April than in May and July for all these source regions with profiles systematically located to the left of the mean line. In addition, non-zero extinctions can only be seen below the 3.5 km in September because the low boundary layer height efficiently inhibited the vertical transport of dust aerosols after emissions. Aerosol signals are frequently influenced by the solar illumination during the daytime, so a higher quality threshold is applied for the data processing, resulting in much less amounts of dust events than during the nighttime. Because of this, the mean extinction during the daytime is stronger and noisier relative to that during the nighttime.

Figure 14 shows scatter plots of the layer-integrated color ratio (χ_{layer}) against the layer-integrated depolarization ratio (δ_{layer}), which are related to the particle shape and size, respectively, and thus are often used to subtype aerosol features in the CALIPSO classification algorithm [45] for the selected dust cases. The depolarization ratio is defined as the ratio between the perpendicular and parallel backscattering at 532 nm. The color ratio is defined as the ratio of the backscattering at 1,064 nm and 532 nm. We calculated the layer-integrated depolarization and color ratio following formula 1 and 2, respectively,

$$\delta_{layer} = \sum_{k=1}^{K} \frac{\beta_{532,\perp,k}}{\beta_{532,\parallel,k}}, \quad (1)$$

$$\chi_{layer} = \sum_{k=1}^{K} \frac{\beta_{1064,k}}{\beta_{532,k}}, \quad (2)$$

where K is the altitude index indicating the top of the dust layer derived from CALIPSO 5 km aerosol layer products; $\beta_{532,\perp,k}$ and $\beta_{532,\parallel,k}$ are the backscattering intensity of perpendicular and parallel components at 532 nm, respectively; $\beta_{1064,k}$ and $\beta_{532,k}$ are the total backscattering intensity at 1,064 and 532 nm.

Preprints (www.preprints.org) | NOT PEER-REVIEWED | Posted: 11 June 2018 doi:10.20944/preprints201806.0158.v1

Peer-reviewed version available at Atmosphere 2018, 9, 288; doi:10.3390/atmos9080288

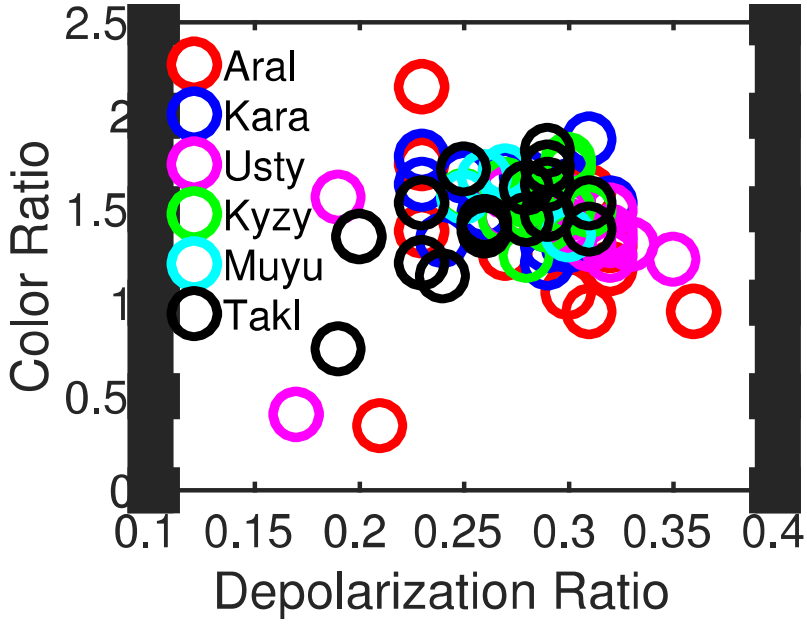

622

623 **Figure 14.** The scatter plot of the layer-integrated color ratio against the layer-integrated
624 depolarization ratio.

625 According to the selected cases, dust particles over the western part of Central Asia tend to be
626 coarser than over the Taklimakan Desert. Excluding extreme cases, the layer-integrated color ratio
627 ranges 1.23 to 2.15 (median: 1.48; mean: 1.49) and 1.14 to 1.81 (median: 1.46; mean: 1.49) for the
628 western part of Central Asia and the Taklimakan Desert, respectively. Extreme cases were seen on
629 September 13 over the Ustyurt and September 15 over the Aral Sea basin. The layer-integrated color
630 ratio is only 0.4 and 0.34, respectively, which are much smaller comparing with other episodes,
631 indicating finer dust aerosols. These extremely low values can be explained by the large dust plume
632 height, as coarse particles are readily deposited onto the ground because of the gravitational settling
633 process and only particles in small sizes can be transported to a higher level. In fact, the layer base
634 heights for these two cases are approximately 2.61 km and 4.49 km, respectively, much larger in
635 comparison to that for other episodes with the plume base close to the surface. A typical dust
636 depolarization ratio is approximately 0.2-0.3, as suggested by Gautam et al. [46]. For Central Asia, the
637 layer-integrated depolarization ratio is greater than 0.2 for most dust episodes except two, one (~0.17)
638 during the nighttime on September 13 over the Ustyurt Plateau and the other one (~0.19) on October
639 15 over the Taklimakan Desert. The median (mean) for the western part of Central Asia is 0.28 (0.29)
640 a little bit larger than for the Taklimakan Desert 0.26 (0.26). The maximum layer-integrated
641 depolarization ratio reaches up to 0.36, much larger than the threshold value 0.2 used by ground-
642 based lidars to identify clouds [47], for dust episodes that occurred on July 15 and September 5 over
643 the Ustyurt Plateau and the Aral Sea, respectively. Coincidentally, this episode is also the one that
644 has the smallest layer-integrated color ratio, indicating a majority of dust particles with non-spherical
645 shape but in small size.

646 **6. Discussion and Conclusions**

647 In this study, four aerosol products from SeaWiFS, MISR, and MODIS onboard Terra and Aqua
648 was analyzed during 2000 – 2016 to investigate the annual and seasonal variability of dust aerosols
649 over Central Asia. DOD was derived from original AOD based on three criterions utilizing the
650 relationship between the particle size and Angstrom exponent. High DOD derived from the four
651 sensors (MODIS onboard Terra and Aqua, SeaWiFS, and MISR) is mainly found over the Taklimakan
652 Desert, the Ustyurt Plateau, the Aral Kum Desert, and the astern Kara Kum Desert near the boundary
653 of Turkmenistan and Uzbekistan, although horizontal extensions surrounding these areas exhibit a
654 clear year-to-year variation. A one-sided Wilcoxon sum rank test on the null hypothesis of equal

median distributions among the spring, summer, and fall seasons was performed to explore whether there is a statistically significant seasonal variation in the satellite-derived DOD with the best estimation quality flag.

Our analysis on the seasonal dynamics suggested that both DOD and dust occurrence derived from satellite multi-sensor observations is insensitive to the selection of the AEt (Table 2). This finding, firstly, indicates the dominance of mineral dust in Central Asia and secondly provides evidence that no considerable differences on derived DOD should be yielded, particularly if results are achieved on seasonal basis, with different AEt values utilized by the scientific community [38,39], as aforementioned references [40]. Significantly higher dust activities were found in the spring in terms of both DOD and dust occurrences under all AEt values over the Taklimakan Desert, but for the western part of Central Asia, the spring season had significantly more frequent dust occurrences, whereas the summer season tends to have statistically larger AOD, albeit disagreement appears among different sensors (e.g., MODIS/Terra) (Table 1 and 4). It is very likely that the dust event in the summer has a higher intensity, releasing a greater number of particles on average than in the spring. Using in site measurements on dust depositions, however, Groll et al. [10] found the most dust is deposited during summer months, particularly in June, when the highest dust frequency is also registered. We realized that the frequency they calculated is based on a medical indicated threshold value 10.5 g m^{-2}. Our previous analysis (Figure 11 and Table 4) has shown that the distribution of the calculated dust occurrence with respect to months is insensitive to DODt and AEt values that are selected and no evident differences on the distribution are seen over the three sub-regions that are located in the western part of Central Asia. The disagreement on the month with the maximum dust occurrence (frequency), thus, might not be explained by the different sub-regions and the threshold values that are used. It is reasonable to argue that their measurement mainly contains coarser dust particles (for instance, dust diameter >8 μm), which tends to deposit due to the gravitational settling mechanism during transport. The unevenly distributed deposition explains the difference, although we cannot exclude other possible reasons associated with the retrieval bias.

DOD is a measure of the dust loading in the atmosphere. Most dust aerosols are deposited onto the ground without experiencing long-range transport. So, the derived DOD in this region can be regarded as mainly a result of local emissions, albeit some areas like Kyrgyzstan might be influenced by the transport of dust aerosols from deserts in Middle East [48]. The dust emission process is mainly controlled by the combination of the soil characteristics like the surface roughness, the soil moisture, the vegetation presence etc. and regional meteorological conditions mainly the wind velocity. The deserts in Central Asia are characterized as a continental climate region. Most precipitation and the green growing are registered in springs associated with the northward migration of the Iranian branch of the Polar front [49]. The average July temperature and maximum temperatures are 32 ℃ and 52 ℃, respectively, in the eastern Kara Kum [49]. The high near-surface temperature and dryness in the summer leading to a reduction of the soil moisture content and the surface covers, which are two main factors that prevent the soil from erosion, very likely contribute to the strong dust emissions [50]. The seasonal surface vegetation dynamics for the Taklimakan Desert is much less evident than for the western part of Central Asia, as can be seen from Figure 3 of Li and Sokolik [4]. Therefore, the seasonal variability of DOD is greatly possible a direct result from changes of the aridity and surface winds induced by the atmospheric patterns like the Siberian Highs and Arctic anticyclones instead of the surface roughness. The peak of DOD and dust occurrences in the spring from the satellite perspective is also supported by results from Xuan and Sokolik [51] and Laurent et al. [52] over the Taklimakan. The decreasing trend of DOD might be explained by the increase of greenings [53] due to the more abundant CO2 concentration, which can increase the photosynthetic rate and reduce water loss through decreasing the stomatal opening.

Differences of AOD and DOD derived from multiple sensors are evident over the Taklimakan Desert and the western part of Central Asia. MISR and SeaWiFS yield significantly lower DOD in comparison to MODIS onboard Terra/Aqua, particularly over the Taklimakan Desert, as can be

clearly seen in Figure S1 and S2. The reason for the significant difference is complex. Take MODIS and MISR for example. In general, there are not too many coincident samplings of MISR and MODIS on the daily basis. On the monthly basis, however, the coincident sampling could be found over much of the research domain (Figure 2 and 4), although the narrow swath width of MISR leads to a much less sampling volume in the interested domain by MISR than by MODIS (Figure 3). MISR AOD is systematically lower than MODS AOD of collection 6 for AOD greater than 0.2 or 0.3 but higher for low AOD. This phenomenon also appears when MODIS AOD of collection 5 is used instead [54]. Due to a lack of ground-based observations, the bias might exist in all these sensors in this region. In fact, previous study [55] has found that MISR slightly underestimated AOD over land whereas MODIS with the dark target algorithm generally overestimated it in comparison to AERONET. The performance of collection 6 with the deep blue algorithm is similar to that of collection 5 over selected AERONET sites and both have larger uncertainties for low and high-AOD conditions [17]. The slight difference in MISR and MODIS spectral bandpasses, with the effective wavelengths of 557.5 and 553.7 nm, respectively, should unlikely cause a significant impact on the AOD retrievals [56]. In addition, MISR set an upper boundary 3 to avoid a huge data volume. MISR tends to show lower AOD/DOD in comparison to MODIS for large-size aerosols (mineral dust) (Figure S3). This behavior arises likely due to the different aerosol optical properties from aerosol models that are used by MODIS and MISR. Models with stronger absorption ability need higher DOD to fit the observed radiance at TOA. The difference in AOD/DOD/occurrences arises mainly due to differences in the spatial coverage, the pixel resolution and the retrieval algorithm, for instance the cloud masking, the radiometric calibration, aerosol models, and surface model assumptions that are used to make aerosol retrievals. More comprehensive comparisons between MODIS and MISR retrievals are available in Kahn et al. [56] over both oceans and lands for MODIS aerosol products with the dark target algorithm. Significant efforts on investigating these factors are needed to explain the difference among multiple sensors.

Analysis on the CALIPSO aerosol product for 83 events in 2007 suggest that dust plumes have multiple structures and are mainly distributed from the surface to the 4-km height with a few episodes over the Taklimakan Desert extending to the top troposphere. A little bit coarser dust particles were found over the western part of Central Asia in comparison to the Taklimakan Desert. No significant differences in particle shape and size are found among sub-regions in the western Central Asia area. In contrast, differences of these physical properties and of the vertical extinction profile are evident among the selected events, likely resulting from varied meteorological conditions that generate the dust emission. Dust aerosols uplifted from desert regions greatly enhance the aerosol extinction near the surface to a higher altitude (Figure 13) due to the vertical transportation. However, we are not aware of any cases with dust aerosols from western Central Asia that can have a long-range transport possibly because of the blocking of the high topography to the south and east (Figure 1), whereas the long-range transport for the Asian dust is well known [23,57-59].The weaker mean extinction of dust plume is consistent to smaller AOD/DOD as suggested by multiple passive sensors over the western part of Central Asia than over the Taklimakan Desert region. Dust aerosols near the Taklimakan Desert are much closer to crustal materials. In contrast, polluted dust either internally-mixed with non-mineral materials [10,44] or externally-mixed with smoke is often detected by CALIPSO over the western part of Central Asia and only a few episodes have the dust plume base away from the surface showing a different size distribution with much finer aerosols (Figure 14). Because the vertical extension of dust plume, particularly relative to clouds [26], the size distribution and chemical compositions primarily mineral oxides [35,60] are crucial factors determining the radiative effects the radiative effects by mineral dust thus might be different between the western part of Central Asia and the Taklimakan Desert, although the shape and size of detected particles are similar.

Supplementary Materials: The following are available online at www.mdpi.com/xxx/s1, Figure S1: Comparisons of AOD (a and e) and DOD (b, c, d, f, g, and h) from MISR, SeaWiFS, and MODIS onboard Aqua with those from MODIS onboard Terra over the Taklimakan Desert on daily basis. Panels b) and f) for criterion

1; Panels c) and g) for criterion 2; Panels d) and h) for criterion 3. Top panels: all quality flags; Bottom panels: the best estimate. Also shown are correlation co-efficiencies and root mean square errors for MISR (red), SeaWiFS (blue), and Aqua (purple). Dash lines indicate the 1:1 lines. Figure S2: Same as Figure S1, but on monthly basis. Figure S3. Differences AOD between MISR (red) / SeaWiFS (blue) / Aqua (purple) and Terra with all quality flags (a and c) and the best estimation (b and d) against the Angstrom exponent from Terra.

Author Contributions: Conceptualization, L.L. and I.N.S.; Methodology, L.L. and I.N.S.; Visualization, L.L. Investigation, L.L.; Writing-Original Draft Preparation, L.L.; Writing-Review & Editing, L.L. and I.N.S.;

please turn to the CRediT taxonomy for the term explanation. Authorship must be limited to those who have contributed substantially to the work reported.

Funding: This research was funded by the NASA Goddard Space and Flight Center grant number [3506c69].

Acknowledgments: This work has been funded by NASA Radiation Program. The MODIS data were obtained through the NASA Goddard Space and Flight Center Data Center Atmosphere Archive and Distribution System (https://ladsweb.nascom.nasa.gov). The MISR data are available through the Jet Propulsion Laboratory website (https://www-misr.jpl.nasa.gov). OMI AAI was obtained through this link https://disc.sci.gsfc.nasa.gov. The CALIPSO data used in this study were obtained from the NASA Langley Atmospheric Science Data Center (https://eosweb.larc.nasa.gov/project/calipso). We also acknowledge all anonymous reviewers for their helpful comments that improve the original manuscript.

Conflicts of Interest: The authors declare no conflict of interest.

References

1. Sokolik, I.N.; Toon, O.B. Direct radiative forcing by anthropogenic airborne mineral aerosols. Nature 1996, 381, 681-683.
2. Jickells, T.D.; An, Z.S.; Andersen, K.K.; Baker, A.R.; Bergametti, G.; Brooks, N.; Cao, J.J.; Boyd, P.W.; Duce, R.A.; Hunter, K.A., et al. Global iron connections between desert dust, ocean biogeochemistry, and climate. Science 2005, 308, 67-71.
3. Atkinson, J.D.; Murray, B.J.; Woodhouse, M.T.; Whale, T.F.; Baustian, K.J.; Carslaw, K.S.; Dobbie, S.; O'Sullivan, D.; Malkin, T.L. The importance of feldspar for ice nucleation by mineral dust in mixed-phase clouds (vol 498, pg 355, 2013). Nature 2013, 500, 491-491.
4. Li, L.L.; Sokolik, I.N. Developing a dust emission procedure for central asia. Air Soil Water Res 2017, 10, 1-12.
5. Saiko, T.A.; Zonn, I.S. Irrigation expansion and dynamics of desertification in the circum-aral region of central asia. Appl Geogr 2000, 20, 349-367.
6. Indoitu, R.; Kozhoridze, G.; Batyrbaeva, M.; Vitkovskaya, I.; Orlovsky, N.; Blumberg, D.; Orlovsky, L. Dust emission and environmental changes in the dried bottom of the aral sea. Aeolian Res 2015, 17, 101-115.
7. Ge, Y.X.; Abuduwaili, J.; Ma, L.; Liu, D.W. Temporal variability and potential diffusion characteristics of dust aerosol originating from the aral sea basin, central asia. Water Air Soil Poll 2016, 227.
8. Orlovsky, L.; Orlovsky, N.; Durdyev, A. Dust storms in turkmenistan. J Arid Environ 2005, 60, 83-97.
9. Orlovsky, N.; Birnbaum, E.H. The role of haloxylon species for combating desertification in central asia. Plant Biosyst 2002, 136, 233-240.
10. Groll, M.; Opp, C.; Aslanov, I. Spatial and temporal distribution of the dust deposition in central asia - results from a long term monitoring program. Aeolian Res 2013, 9, 49-62.
11. Mahowald, N.M.; Dufresne, J.L. Sensitivity of toms aerosol index to boundary layer height: Implications for detection of mineral aerosol sources. Geophys Res Lett 2004, 31.

12. Papadimas, C.D.; Hatzianastassiou, N.; Mihalopoulos, N.; Querol, X.; Vardavas, I. Spatial and temporal variability in aerosol properties over the mediterranean basin based on 6-year (2000-2006) modis data. J Geophys Res-Atmos 2008, 113.
13. Kosmopoulos, P.G.; Kaskaoutis, D.G.; Nastos, P.T.; Kambezidis, H.D. Seasonal variation of columnar aerosol optical properties over athens, greece, based on modis data. Remote Sens Environ 2008, 112, 2354-2366.
14. Martonchik, J.V.; Diner, D.J.; Kahn, R.; Gaitley, B.; Holben, B.N. Comparison of misr and aeronet aerosol optical depths over desert sites. Geophys Res Lett 2004, 31.
15. Christopher, S.A.; Wang, J. Intercomparison between multi-angle imaging spectroradiometer (misr) and sunphotometer aerosol optical thickness in dust source regions over china: Implications for satellite aerosol retrievals and radiative forcing calculations. Tellus B 2004, 56, 451-456.
16. Liu, J.; Xia, X.; Li, Z.; Wang, P.; Min, M.; Hao, W.; Wang, Y.; Xin, J.; Li, X.; Zheng, Y., et al. Validation of multi-angle imaging spectroradiometer aerosol products in china. Tellus B 2010, 62, 117-124.
17. Sayer, A.M.; Hsu, N.C.; Bettenhausen, C.; Jeong, M.J. Validation and uncertainty estimates for modis collection 6 "deep blue" aerosol data. J Geophys Res-Atmos 2013, 118, 7864-7872.
18. Hsu, N.C.; Tsay, S.C.; King, M.D.; Herman, J.R. Aerosol properties over bright-reflecting source regions. Ieee T Geosci Remote 2004, 42, 557-569.
19. Ginoux, P.; Garbuzov, D.; Hsu, N.C. Identification of anthropogenic and natural dust sources using moderate resolution imaging spectroradiometer (modis) deep blue level 2 data. J Geophys Res-Atmos 2010, 115.
20. Prospero, J.M.; Ginoux, P.; Torres, O.; Nicholson, S.E.; Gill, T.E. Environmental characterization of global sources of atmospheric soil dust identified with the nimbus 7 total ozone mapping spectrometer (toms) absorbing aerosol product. Rev Geophys 2002, 40.
21. Kaskaoutis, D.G.; Kambezidis, H.D.; Nastos, P.T.; Kosmopoulos, P.G. Study on an intense dust storm over greece. Atmos Environ 2008, 42, 6884-6896.
22. Schepanski, K.; Tegen, I.; Macke, A. Comparison of satellite based observations of saharan dust source areas. Remote Sens Environ 2012, 123, 90-97.
23. Huang, J.; Minnis, P.; Chen, B.; Huang, Z.W.; Liu, Z.Y.; Zhao, Q.Y.; Yi, Y.H.; Ayers, J.K. Long-range transport and vertical structure of asian dust from calipso and surface measurements during pacdex. J Geophys Res-Atmos 2008, 113.
24. Liu, Z.Y.; Omar, A.; Vaughan, M.; Hair, J.; Kittaka, C.; Hu, Y.X.; Powell, K.; Trepte, C.; Winker, D.; Hostetler, C., et al. Calipso lidar observations of the optical properties of saharan dust: A case study of long-range transport. J Geophys Res-Atmos 2008, 113.
25. Liao, H.; Seinfeld, J.H. Radiative forcing by mineral dust aerosols: Sensitivity to key variables. J Geophys Res-Atmos 1998, 103, 31637-31645.
26. Quijano, A.L.; Sokolik, I.N.; Toon, O.B. Radiative heating rates and direct radiative forcing by mineral dust in cloudy atmospheric conditions. J Geophys Res-Atmos 2000, 105, 12207-12219.
27. Meloni, D.; di Sarra, A.; Di Iorio, T.; Fiocco, G. Influence of the vertical profile of saharan dust on the visible direct radiative forcing. J Quant Spectrosc Ra 2005, 93, 397-413.
28. Tulet, P.; Mallet, M.; Pont, V.; Pelon, J.; Boone, A. The 7-13 march 2006 dust storm over west africa: Generation, transport, and vertical stratification. J Geophys Res-Atmos 2008, 113.

29. Gkikas, A.; Hatzianastassiou, N.; Mihalopoulos, N.; Torres, O. Characterization of aerosol episodes in the greater mediterranean sea area from satellite observations (2000-2007). Atmos Environ 2016, 128, 286-304.
30. Hamonou, E.; Chazette, P.; Balis, D.; Dulac, F.; Schneider, X.; Galani, E.; Ancellet, G.; Papayannis, A. Characterization of the vertical structure of saharan dust export to the mediterranean basin. J Geophys Res-Atmos 1999, 104, 22257-22270.
31. Ansmann, A.; Baars, H.; Tesche, M.; Muller, D.; Althausen, D.; Engelmann, R.; Pauliquevis, T.; Artaxo, P. Dust and smoke transport from africa to south america: Lidar profiling over cape verde and the amazon rainforest. Geophys Res Lett 2009, 36.
32. Adams, A.M.; Prospero, J.M.; Zhang, C.D. Calipso-derived three-dimensional structure of aerosol over the atlantic basin and adjacent continents. J Climate 2012, 25, 6862-6879.
33. Eguchi, K.; Uno, I.; Yumimoto, K.; Takemura, T.; Shimizu, A.; Sugimoto, N.; Liu, Z. Trans-pacific dust transport: Integrated analysis of nasa/calipso and a global aerosol transport model. Atmos Chem Phys 2009, 9, 3137-3145.
34. Indoitu, R.; Orlovsky, L.; Orlovsky, N. Dust storms in central asia: Spatial and temporal variations. J Arid Environ 2012, 85, 62-70.
35. Li, L.; Sokolik, I.N. The dust direct radiative impact and its sensitivity to the land surface state and key minerals in the wrf-chem-dumo model: A case study of dust storms in central asia. J Geophys Res-Atmos 2018, 123.
36. Mishchenko, M.I.; Travis, L.D.; Kahn, R.A.; West, R.A. Modeling phase functions for dustlike tropospheric aerosols using a shape mixture of randomly oriented polydisperse spheroids. J Geophys Res-Atmos 1997, 102, 16831-16847.
37. Torres, O.; Tanskanen, A.; Veihelmann, B.; Ahn, C.; Braak, R.; Bhartia, P.K.; Veefkind, P.; Levelt, P. Aerosols and surface uv products from ozone monitoring instrument observations: An overview. J Geophys Res-Atmos 2007, 112.
38. Ginoux, P.; Prospero, J.M.; Gill, T.E.; Hsu, N.C.; Zhao, M. Global-scale attribution of anthropogenic and natural dust sources and their emission rates based on modis deep blue aerosol products. Rev Geophys 2012, 50.
39. Schepanski, K.; Tegen, I.; Laurent, B.; Heinold, B.; Macke, A. A new saharan dust source activation frequency map derived from msg-seviri ir-channels. Geophys Res Lett 2007, 34.
40. Xu, Y. Evaluation of mineral dust aerosol optical depth and related components from the chimere-dust model using satellite remote sensing and ground-based observations. Atmos Environ 2018.
41. Ciren, P.; Kondragunta, S. Dust aerosol index (dai) algorithm for modis. J Geophys Res-Atmos 2014, 119, 4770-4792.
42. Darmenova, K.; Sokolik, I.N.; Shao, Y.P.; Marticorena, B.; Bergametti, G. Development of a physically based dust emission module within the weather research and forecasting (wrf) model: Assessment of dust emission parameterizations and input parameters for source regions in central and east asia. J Geophys Res-Atmos 2009, 114.
43. Baddock, M.C.; Ginoux, P.; Bullard, J.E.; Gill, T.E. Do modis-defined dust sources have a geomorphological signature? Geophys Res Lett 2016, 43, 2606-2613.
44. Razakov, R.M.; Kosnazarov, K.A. Dust and salt transfer from the exposed bed of the aral sea and measures to decrease its environmental impact. In NATO ASI Series (Series 2. Environment), Micklin, P.P.; Williams, W.D., Eds. Springer: Berlin, Heidelberg, 1996; Vol. 12, pp 95-102.

45. Omar, A.H.; Winker, D.M.; Kittaka, C.; Vaughan, M.A.; Liu, Z.Y.; Hu, Y.X.; Trepte, C.R.; Rogers, R.R.; Ferrare, R.A.; Lee, K.P., et al. The calipso automated aerosol classification and lidar ratio selection algorithm. J Atmos Ocean Tech 2009, 26, 1994-2014.
46. Gautam, R.; Liu, Z.Y.; Singh, R.P.; Hsu, N.C. Two contrasting dust-dominant periods over india observed from modis and calipso data. Geophys Res Lett 2009, 36.
47. Shimizu, A.; Sugimoto, N.; Matsui, I.; Arao, K.; Uno, I.; Murayama, T.; Kagawa, N.; Aoki, K.; Uchiyama, A.; Yamazaki, A. Continuous observations of asian dust and other aerosols by polarization lidars in china and japan during ace-asia. J Geophys Res-Atmos 2004, 109.
48. Chen, B.B.; Sverdlik, L.G.; Imashev, S.A.; Solomon, P.A.; Lantz, J.; Schauer, J.J.; Shafer, M.M.; Artamonova, M.S.; Carmichael, G.R. Lidar measurements of the vertical distribution of aerosol optical and physical properties over central asia. International Journal of Atmospheric Sciences 2013, 2013, 1-17.
49. Lioubimtseva, E.; Cole, R.; Adams, J.M.; Kapustin, G. Impacts of climate and land-cover changes in arid lands of central asia. J Arid Environ 2005, 62, 285-308.
50. Xi, X.; Sokolik, I.N. Seasonal dynamics of threshold friction velocity and dust emission in central asia. J Geophys Res-Atmos 2015, 120, 1536-1564.
51. Xuan, J.; Sokolik, I.N. Characterization of sources and emission rates of mineral dust in northern china. Atmos Environ 2002, 36, 4863-4876.
52. Laurent, B.; Marticorena, B.; Bergametti, G.; Mei, F. Modeling mineral dust emissions from chinese and mongolian deserts. Global Planet Change 2006, 52, 121-141.
53. de Beurs, K.M.; Henebry, G.M.; Owsley, B.C.; Sokolik, I. Using multiple remote sensing perspectives to identify and attribute land surface dynamics in central asia 2001-2013. Remote Sens Environ 2015, 170, 48-61.
54. Kahn, R.A.; Garay, M.J.; Nelson, D.L.; Yau, K.K.; Bull, M.A.; Gaitley, B.J.; Martonchik, J.V.; Levy, R.C. Satellite-derived aerosol optical depth over dark water from misr and modis: Comparisons with aeronet and implications for climatological studies. J Geophys Res-Atmos 2007, 112.
55. Abdou, W.A.; Diner, D.J.; Martonchik, J.V.; Bruegge, C.J.; Kahn, R.A.; Gaitley, B.J.; Crean, K.A.; Remer, L.A.; Holben, B. Comparison of coincident multiangle imaging spectroradiometer and moderate resolution imaging spectroradiometer aerosol optical depths over land and ocean scenes containing aerosol robotic network sites. J Geophys Res-Atmos 2005, 110.
56. Kahn, R.A.; Nelson, D.L.; Garay, M.J.; Levy, R.C.; Bull, M.A.; Diner, D.J.; Martonchik, J.V.; Paradise, S.R.; Hansen, E.G.; Remer, L.A. Misr aerosol product attributes and statistical comparisons with modis. Ieee T Geosci Remote 2009, 47, 4095-4114.
57. Uno, I.; Amano, H.; Emori, S.; Kinoshita, K.; Matsui, I.; Sugimoto, N. Trans-pacific yellow sand transport observed in april 1998: A numerical simulation. J Geophys Res-Atmos 2001, 106, 18331-18344.
58. Liu, Z.Y.; Sugimoto, N.; Murayama, T. Extinction-to-backscatter ratio of asian dust observed with high-spectral-resolution lidar and raman lidar. Appl Optics 2002, 41, 2760-2767.
59. Uno, I.; Eguchi, K.; Yumimoto, K.; Takemura, T.; Shimizu, A.; Uematsu, M.; Liu, Z.Y.; Wang, Z.F.; Hara, Y.; Sugimoto, N. Asian dust transported one full circuit around the globe. Nat Geosci 2009, 2, 557-560.
60. Sokolik, I.N.; Toon, O.B. Incorporation of mineralogical composition into models of the radiative properties of mineral aerosol from uv to ir wavelengths. J Geophys Res-Atmos 1999, 104, 9423-9444.